A PI(3,5)P2 probe reveals PIKfyve is required for Rab7 acquisition and the delivery and fusion of early macropinosomes to phagosomes

James H. Vines[1], Catherine M. Buckley[1,4], Hannes Maib[2], Aurelie Gueho[3], Thierry Soldati[3], David Murray[2] and Jason S. King[1*]

[1]School of Biosciences, University of Sheffield, Firth Court Western Bank, Sheffield, UK.
[2]Division of Cell and Developmental Biology, School of Life Sciences, University of Dundee.
[3]Department of Biochemistry, Faculty of Sciences, University of Geneva, Switzerland.
[4]Current address: Department of Medicine, Cambridge University, UK.

[*]Corresponding author: Jason.King@sheffield.ac.uk

Keywords: Phagocytosis, PIKfyve, *Dictyostelium*, phosphatidylinositol(3,5)-bisphosphate, macropinocytosis.

Abstract

Phosphoinositide signalling lipids (PIPs) are key regulators of membrane identity and vesicle trafficking. Of these, PI(3,5)P2 is one of the least understood, despite key roles in many endocytic pathways including phagocytosis and macropinocytosis. PI(3,5)P2 is predominantly generated by the phosphoinositide 5-kinase PIKfyve, and is critical for phagosomal digestion and the killing of engulfed microbes. However, the regulation of PIKfyve activity, PI(3,5)P2 dynamics, and how they control phagosome maturation remains unclear. Using the model professional phagocyte *Dictyostelium discoideum* we have identified a highly selective PI(3,5)P2-binding protein that allows faithful observation of PI(3,5)P2 dynamics in live cells. Using this probe we demonstrate that PIKfyve recruitment and activity are separable, and that PIKfyve activation stimulates its own dissociation from membranes. We show that PI(3,5)P2 accumulates on phagosomes 2-3 minutes after engulfment drives fusion of a specific population of PI(3,5)P2 and Rab7-positive macropinosomes. We find PIKfyve is required for the fusion between macropinosomes and phagosomes, which enables phagosomes to efficiently accumulate Rab7 and other components of the lysosomal machinery. These findings uncover key mechanistic details of the role and regulation of PIKfyve/PI(3,5)P2 likely to have general relevance across endocytic pathways.

Introduction

The inositol phospholipids are a family of interconvertible signals that define distinct endocytic compartments. Differential phosphorylation at three positions on the inositol headgroup allows seven different signalling species to be generated. These are used to recruit specific effector proteins to membranes and are interconverted by a large family of lipid kinases and phosphatases. Transitions between different phosphoinositides (PIPs) are thus central components of the identity, sorting and progression of almost all membrane compartments.

One of the least understood PIP transitions is the generation of PI(3,5)P2 by the phosphoinositide 5-kinase PIKfyve (Fab1p in yeast). PIKfyve is recruited to early endosomes via its FYVE (Fab1, YOTB, Vac1 and EEA1) domain that binds PI(3)P and subsequently phosphorylates it at the 5-position to produce PI(3,5)P2 (Cabezas et al., 2006; Sbrissa et al., 1999; Yamamoto et al., 1995). PIKfyve is in a complex with the scaffolding regulator Vac14 (ArPIKfyve) and the 5-phosphatase Fig4 (Sac3) which catalyses the reverse reaction (Botelho et al., 2008; Rudge et al., 2004; Sbrissa et al., 2007). This complex is under intricate regulation, and whilst genetic, biochemical and structural studies have provided some mechanistic insight (Berwick et al., 2004; Ikonomov et al., 2009; Lees et al., 2020; Sbrissa et al., 2000), the dynamics of PI(3,5)P2 formation *in vivo* have remained elusive due to the lack of a reliable live-cell reporter.

Disruption of PIKfyve causes severe and widespread defects in endocytic trafficking in all organisms studied, typified by the formation of swollen endosomes and defects in lysosomal degradation (Buckley et al., 2019; Choy et al., 2018; de Lartigue et al., 2009; Dove et al., 2009; Ikonomov et al., 2001; Kim et al., 2014; Krishna et al., 2016; Nicot et al., 2006). PIKfyve activity is therefore critical for several physiologically important pathways such as the digestion by autophagosomes, phagosomes and of endocytosed receptors (Buckley et al., 2019; de Lartigue et al., 2009; Demirsoy et al., 2017; Ferguson et al., 2009; Kim et al., 2014; McCartney et al., 2014b; Rusten et al., 2006). Unsurprisingly, disrupted PI(3,5)P2 signalling is implicated in a broad range of diseases (reviewed in (McCartney et al., 2014a; Shisheva, 2012).

How these phenotypes result from PI(3,5)P2 deficiency is not clear. Several studies have indicated that PI(3,5)P2 can directly regulate lysosomal ion channels such as mucolipin (TRPML), Two-Pore calcium channels (TPCs), and the chloride channel ClC7 (Dong et al., 2010; Leray et al., 2022; Samie et al., 2013; Wang et al., 2012). PI(3,5)P2 has also been shown to regulate association of the two vacuolar ATPase (V-ATPase) subcomplexes on the yeast vacuole, although this has not yet been confirmed in other organisms (Li et al., 2014). Loss of PI(3,5)P2 can also affect lysosomal transport and delivery to the compartments targeted for degradation (Li et al., 2016). Each mechanism can potentially contribute to the phenotypes observed, but our understanding is limited by poor knowledge of where and when PI(3,5)P2 is generated.

The lack of a reliable reporter is perhaps the biggest limitation in understanding the function of PI(3,5)P2 and the regulation of the enzymes that generate it. Whilst a tandem repeat of the N-terminal lipid-binding region of TRPML showed PI(3,5)P2 specificity *in vitro* and looked promising in cells (Li et al., 2013), others found clear evidence of non-specific endosomal recruitment and retention after PI(3,5)P2 depletion (Hammond et al., 2015). Therefore, one of the major aims of this study was to identify and validate an alternative reporter to faithfully describe PI(3,5)P2 dynamics within live cells.

We and others have previously demonstrated a key role for PIKfyve during phagosome maturation. Phagocytosis is the endocytic pathway used by cells to engulf large extracellular particles such as microbes, dead cells and debris. This is highly related to the process of macropinocytosis, whereby cells take up extracellular fluid to feed or sample their environment (King and Kay, 2019). Upon ingestion, phagocytes must rapidly process and kill any engulfed microbes to protect from infection. Phagosomes follow a complex maturation pathway to recycle surface proteins before they get digested and then deliver an array of antimicrobial and digestive components to defend against potential pathogens (Buckley et al., 2016; Chen et al., 2010; Levin et al., 2016). Like other endocytic pathways, the progression of phagosome maturation is also regulated by the sequential exchange of key signalling molecules on the phagosomal membrane such as PIPs and the Rab family of small GTPases (Gutierrez, 2013; Smith et al., 2007).

Using the well characterised amoeba *Dictyostelium discoideum* as a model professional phagocyte, we previously found cells lacking PIKfyve had severe defects in delivering

lysosomal enzymes to phagosomes (Buckley et al., 2019). *PIKfyve*-null cells are defective in phagosomal proteolysis and killing, rendering them hypersensitive to infection with *Legionella pneumophila*, and demonstrating the physiological importance of PIKfyve in innate immunity. PIKfyve is also important for phagosome-lysosome fusion in both macrophages and neutrophils (Dayam et al., 2015; Dayam et al., 2017; Isobe et al., 2019; Kim et al., 2014). This indicates a central and conserved role, but how PIKfyve activity is regulated and integrates with other components of the phagosomal maturation machinery such as Rab signalling and fusion with other endosomal compartments is poorly understood.

Here, we investigate the role and regulation of PIKfyve in *Dictyostelium* phagosome maturation. We find that whilst PIKfyve-deficient phagosomes can acquire and recycle Rab5, they accumulate almost no Rab7, which is normally delivered by vesicle fusion. We identify and characterise SnxA - a new highly-selective PI(3,5)P2-binding protein, enabling us to visualise PI(3,5)P2 dynamics during phagosome maturation for the first time. This demonstrates a new level of regulation in both PIKfyve recruitment and activity and uncovers key mechanistic details. Finally, we find PIKfyve has a specific role in regulating heterotypic fusion between phagosomes and a defined population of macropinosomes, which we suggest plays a previously unappreciated role in maintaining digestive efficiency.

Materials and Methods

Dictyostelium Culture

All *Dictyostelium discoideum* cells were derived from the Ax2 (Kay) laboratory strain background unless stated otherwise, and were grown in adherent culture in filter sterilised HL5 medium (Formedium) at 22°C. Cells expressing extrachromosomal plasmids were transformed by electroporation and grown in appropriate antibiotic selection by addition of either 20 µg/ml hygromycin (Invitrogen) or 10 µg/ml G418 (Sigma). PIKfyve knockout strain in Ax2 background generated as previously described (Buckley et al., 2019). Live cell imaging was performed in defined SIH medium (Formedium).

Growth on bacterial lawns was performed by seeding ~20 *Dictyostelium* cells with suspension of *Klebsiella aerogenes* on SM agar plates (Formedium). Colonies were visible after 5 days and colony size measured each day. Tests of growth on a panel of bacteria were performed as described by (Froquet et al., 2009). Dilutions from 1 to 1 x 10^4 cells were seeded on agarose in wells of a 96-well plate containing the relevant bacteria. After several days (dependent on bacterial strain) wells were scored for the presence of *Dictyostelium* colonies. Bacteria used were a gift from Pierre Cosson and were: *K. pneumoniae* laboratory strain and 52145 isogenic mutant (Benghezal et al., 2006), *M. luteus* (Wilczynska and Fisher, 1994), the isogenic *P. aeruginosa* strains PT5 and PT531 (*rhlR-lasR* avirulent mutant) (Cosson et al., 2002), *E. coli* B/r (Gerisch, 1959), non-sporulating *B. subtilis* 36.1 (Ratner and Newell, 1978) and *E.coli* DH5α (Fisher Scientific). An avirulent strain of *K. pneumoniae* was obtained from ATCC (Strain no. 51697).

Cloning

All gene sequences used for cloning were obtained from dictybase (http://www.dictybase.org/) (Fey et al., 2013). A full list of plasmids used is in Table 1. GFP-Rab5A (pJV0054), SnxA-GFP (pJSK619), and PIKfyve-GFP (pJV0025) plasmids were generated by cloning the respective coding sequences from cDNA by PCR using primeSTAR max DNA polymerase (Clontech), subcloning into zero blunt TOPO II vector (Life Technologies) and then cloning into the respective BglII/SpeI sites of the pDM expression plasmid system (Paschke et al., 2018; Veltman et al., 2009). Sequences for the 1xPX-GFP

(pJV0010) and 2xPX-GFP (pJV0016) constructs were synthesised by DC Biosciences. All coding sequences were verified and final plasmids confirmed by restriction digest. 2xFYVE-GFP (pJSK418) uses the sequence from the human Hrs gene and was previously described (Calvo-Garrido et al., 2014). A GFP-Rab7A (pTH70) plasmid was kindly gifted by Huaquing Cai (Tu et al., 2022). Co-expression plasmids were created by first cloning the RFP-fusion sequence into the pDM series shuttle vectors (pDM1042 and pDM1121), before cloning as an NgoMIV fragment into the appropriate GFP-expression vector. The SnxA-GFP integrating vector, was made by cloning full-length SnxA into the integrating C-terminal GFP vector pDM1053 (Paschke et al., 2018). Prior to transformation, the plasmid was linearised with BamHI, and transformation performed with 100 U of BamHI, producing a 5-10 fold increase in the number of colonies compared to controls. Colonies were selected and screened by confocal microscopy for a cell line with low-expression and high contrast. For extrachromosomal expression as an RFP-fusion, a 2xPX construct was used as it gave better contrast. PX domain containing proteins encoded within the *Dictyostelium* genome were identified by BLAST. The genes indicated were then amplified by PCR from cDNA and cloned as above into the GFP-expression vector pDM448.

Generating SnxA knockouts

The SnxA (DDB_G0289833) locus was disrupted by homologous recombination, inserting a blasticidin resistance cassette within the gene and deleting 550 bp of coding sequence. The knockout construct was made using a one-step recombination method into the pKOSG-OBA-Dicty vector as previously described (Wiegand et al., 2011). The 5' recombination arm was generated with the primers agcgcgtctccaatgACCACCCAGGTTAAAAATAATTCC/ agcgcgtctcccttcTTCCTTTTCTAAGAGAATATATTTGG, and the 3' arm with agcgcgtctccgttgCCTTAAAAGAGACGAAGGT/ agcgcgtctcctcccCTGGCTTTGTTTTTATAAAACAG. PCR products were recombined with the vector using StarCombinase (IBA GmbH, Göttingen, Germany). The resulting vector was used to transform Ax2 *Dictyostelium*, and the resulting blasticidin-resistant clones were screened for successful gene disruption by PCR using the primers GCACTGGGAGTTCCAATATCAATATCATC/ ATAATTAATTCAACATCTTGCAAAT. Multiple independent clones were isolated and used for functional characterisation.

Preparation of fluorescent yeast and dextran

Saccharomyces cerevisiae were used for phagocytosis assays. To obtain non-budded yeast, cells were grown for 3 days at 37 °C in standard YPD media (Formedium) until stationary phase. For a budded population, growth was halted while yeast were still in log phase. Both populations were then centrifuged at 1000 x g for 5 minutes and resuspended to a final concentration of $1x10^9$ cells/mL in PBS pH7, then frozen until use. Yeast were fluorescently labelled using either pHrodo red succinimidyl ester (Life Technologies), or Alexa-405 succinimidyl ester (Life Technologies) at a final concentration of 0.25 mM and 2.5 mM, respectively. $0.5x10^9$ yeast were resuspended in 200uL PBS at pH8.5 and incubated with 10uL of prepared dye for 30-minutes at 37 °C with gentle shaking. After, cells were pelleted and sequentially washed in 1 ml of PBS pH 8.5, 1 ml of 25 nM Tris-HCl pH 8.5, and 1 ml of PBS pH 8.5 again. Finally, cells were resuspended in 500 µl of KK2 pH 6.1 and kept at -20°C. Yeast were diluted in SIH to a working concentration of $1x10^8$ yeast/mL before use. Texas-Red 70kDa Dextran (Life Technologies) was resuspended in water and diluted to a working concentration of 2 mg/mL. Far-red dextran was generated by labelling 70kDa dextran (Invitrogen) with Alexa Fluor 680 NHS Ester (Invitrogen) as above, removing unbound dye by dialysis in KK2.

Microscopy and image analysis

For fluorescence microscopy ~1 x 10^6 *Dictyostelium* cells were seeded in 35 mm glass-bottomed microscopy dishes (Mat tek P35G-1.5-14-C), and left to grow overnight in SIH medium (Formedium). Cells were imaged on a Zeiss LSM880 AiryScan Confocal with x63 Plan Apochromat oil objective and processed using the Zeiss microscope software, unless otherwise stated.

For dual colour timelapse phagocytosis assays, most of the medium was aspirated immediately before imaging, and 20 uL of $1x10^8$ dyed yeast added. After 60 seconds, cells were overlaid with a thin layer of 1% agarose in SIH and excess medium removed. For normal timelapses, images were captured every 10 seconds for up to 10 minutes. For extended timelapses, images were captured every 60 s. Automated analysis of the fluorescent intensity around each phagosomal membrane was performed using the Python plugin pyimagej (**Figure S2A-C**). Images where phagosomal entry could be seen were manually selected. To segment out the phagosome, the yeast channel was thresholded and particles larger than $1.5\mu m^2$ selected. Particles on time-adjacent frames were automatically scored for similarity based on position and size, and high similarity particles categorized into the same

event. Then, throughout each event, the phagosome area was monitored for fluorescence change of pHrodo-labelled-yeast as a proxy for phagosomal pH. The selection perimeter was enlarged into two rings of ~0.35 µm thickness: an inner ring 0.2 µm enlarged, to measure enrichment at the phagosomal membrane, and an outer ring 0.85 µm enlarged, to monitor background cytosol fluorescence. Each event was then manually screened for errors before mean fluorescence intensity was recorded for each frame, normalized to intracellular background, and fold enrichment from -10s calculated. Because addition of an agarose overlay appeared to suppress the effects of apilimod, cells treated with 5 µM apilimod (added >2 hours before imaging) (USBiological) were instead imaged without overlay through a larger Z range every 10s using a Nikon W1 Spinning Disk Confocal. The automated analysis pipeline was not sensitive enough to detect PIKfyve-GFP enrichment, so events were manually followed and scored as either GFP positive or negative using ImageJ.

Dextran pulse-chases were performed by aspirating most of the medium, then adding 50 µl of 2 mg/ml 70kDaTexas Red dextran for the indicated time. Dextran was the removed by washing thrice in SIH medium, leaving ~1 ml of SIH in the dish. Cells were immediately imaged, with multiple fields of view taken every 2 minutes for 10 minutes. Macropinosome number and size were quantified automatically using an ImageJ script. GFP colocalisation at each timepoint was scored manually.

For macropinosomes-phagosome fusion assays, 50 uL of 2 mg/ml Texas Red dextran was added to cells for the time indicted for macropinosomes to form. The dish was then washed as above, before addition of 20 uL of $1x10^8$ dyed yeast and then agarose overlay after a further 60 seconds. Clustering analysis was performed using a modified version of the automated analysis pipeline described above. For macropinosome/macropinosome mixing a second dye, 50 uL of Alexa680 70kDa Dextran, was added instead of yeast. For macropinosome/phagosome fusion assays, budded yeast were used instead and analysis of fusion performed manually in ImageJ by measuring the mean intensity across the yeast neck over time. For analysis of clustering macropinosomes, macropinosomes within 1 µm of the phagosome were manually scored as GFP positive or negative, and scored binned into 2-minute intervals.

Western blotting and PIP arrays

Wildtype and ΔPIKfyve cells expressing GFP-Rab5A, GFP-2xFYVE, or GFP-Rab7A were analysed by SDS-PAGE and Western blot using a rabbit anti-GFP primary antibody (gift from Andrew Peden) and a fluorescently conjugated anti-rabbit 800 secondary antibody, using standard techniques. The endogenous biotinylated mitochondrial protein methylcrotonoyl-CoA Carboxylase 1 (MCCC1) was used as a loading control using Alexa680-conjugated streptavadin (Life Technologies) (Davidson et al., 2013). PIP arrays were performed using whole cell lysates from *Dictyostelium* cells expressing the GFP-fusion constructs. ~2 x 10^8 cells were lysed in RIPA buffer (50 mM Tris HCL pH 7.5, 150 mM NaCl, 0.1% SDS, 2 mM EDTA, 0.5 % sodium deoxycholate, 1x HALT protease inhibitor cocktail (Pierce)). PIP arrays (Echelon Biosciences) were blocked for 1 hour at room temperature in 3% fatty acid free BSA in TBS-T, and then incubated with lysates for 1 hour. Membranes were probed with anti-GFP antibody as for Western blots.

Endocyosis and fluid phase proteolysis

Macropinocytosis and exocytosis (Maniak, 2001), by incubating 5 × 10^6 cells/ml in HL5 medium containing 2 mg/ml 70kDa FITC dextran (Sigma). 500 µl of cells was then removed at each timepoint added to 1ml ice-cold KK2 (0.1 M potassium phosphate pH 6.1). Cell pellets were then washed once and lysed in 50 mM Na_2HPO_4 pH 9.3 0.2% Triton X-100 before FITC fluorescence was measured in a fluorimeter. Exocytosis was measured in the same way, except cells were pre-incubated with FITC-dextran for at least 2 hours, before washing out and measuring the decrease in fluorescence over time.

To measure proteolysis of a fluid phase substrate 3 x 10^6 cells/ml were washed twice with LoFlo medium (Formedium). 100 µl of cells (3 x 10^5 cells) was added in triplicate to a 96 well plate and left to attach for 30 minutes. Media was removed from the wells carefully by blotting onto tissue then 100 µl of 0.2 mg/ml DQ-BSA solution (in LoFlo) was added to the wells, except for three wells used to measure the background to which just LoFlo was added. Cells were incubated for 2 minutes then washed thrice before fluorescence was measured on a plate reader (Synergy Mx, Biotek) every 30 s for 15 minutes. Signals were normalised to the maximum signal in Ax2 cells.

Purification of recombinant proteins

All SnxA probes were expressed as N-terminal 6xHis and eGFP fusion proteins in BL21 cells in LB media containing Ampicillin and 1.7 g Lactose per litre for 7 h at 37 °C before lowering down to 18 °C for ~10-12 h. Cells were pelleted and lysed by ultrasound before clearing by centrifugation at 60,000 x *g* for 1 h. Cleared lysates were filtered through a 0.22 µm filter and purified using a 5ml His trap HP column followed by anion exchange using a 5 ml Capto-Q column and size exclusion chromatography using a Superdex 200 16/60 pg column. All probes were snap frozen in liquid nitrogen and stored at -80 °C.

Lipid binding experiments

Performed as previously (Maib and Murray, 2022). 1 mg liposomes, containing each of the seven different phosphatidylinositols were produced by mixing 95 mol percent POPC (1-palmitoyl-2-oleoyl-sn-glycero-3-phosphocholine) with 5 mol % of the respective phosphatidylinositol together with 0.1% Atto647N-DOPE. The mixtures were evaporated under nitrogen and dried overnight in a vacuum extruder. Dried lipids were resuspended in 1ml buffer containing 150 mM NaCl, 20 mM HEPES and 0.5 mM TCEP and subjected to 6 freeze-thaws in liquid nitrogen. Liposomes ~100 nm diameter were generated by passing the lipid mixture 11 times through a 100 nm filter (Whatman Nuclepore). Liposomes were aliquoted, snap frozen and stored at -20 °C.

Membrane coated beads were generated by adding 10 µg of liposomes to ~0.5 x 10^6 10 µm silica beads (Whitehouse Scientific) in 100 µl of 200 mM NaCl for 30min rotation at room temperature. Beads were washed twice and resuspended in buffer containing 150 mM NaCl, 20 mM HEPES, 0.5 mM TCEP (tris(2-carboxyethyl)phosphine hydrochloride) and blocked with 10% goat serum for 30 min. Drops of 7.5µl beads were added into the corners of uncoated µ-Slide 8 well chambers (Ibidi) and 7.5 µl of the purified SnxA probes were added and mixed by pipetting at indicated final concentrations. Lipid binding kinetics were allowed to equilibrate for 30 min at room temperature before imaging close to the equator of the beads.

Confocal images were acquired using a Leica SP8 Confocal Microscope with a Leica HC PL APO CS2 63x/1.40 Oil objective at 0.75 base zoom with 1024x1024 pixels scan. GFP and Atto647N-DOPE fluorescence were imaged simultaneously without any measurable bleed through. Data was analysed using a custom imageJ script that segments the Atto647N-DOPE

channel to create a mask around the outer circumference for each bead. Segmented masks were then used to measure GFP fluorescence around each bead.

Phagocytosis assays

Bead uptake, proteolysis and acidification were performed as previously described in detail in (Sattler et al., 2013). Briefly, phagocytosis was measured by uptake of 1 µm YG-green beads (Polysciences Inc.). Cells were incubated with beads for the times indicated and fluorescence measured by flow cytometry. pH and proteolysis were measured using 3 µm silica beads (Kisker Biotech) conjugated to either FITC or BSA respectively as well as alexa594 as a reference dye. Synchronous phagocytosis was caused by centrifuging beads unto confluent cells in a 96-well plate (1,200 RPM for 10 seconds) before washing and measuring changes in the fluorescence intensities over time. All samples were measured in triplicate.

Statistics

Statistical analysis was performed using Graphpad Prism 9. Biological replicate numbers and statistical tests used for each experiment are detailed in each figure legend. A p-value of <0.05 were deemed significant with * indicating $p<0.05$, **$p<0.01$ and ***$p<0.005$ throughout.

Results

PIKfyve localizes to early phagosomes and macropinosomes

To better understand why PIKfyve disruption inhibits phagosomal maturation, and causes the highly swollen macropinosomes described previously, we first characterised PIKfyve dynamics. Although expression of N-terminally GFP-tagged PIKfyve in wildtype cells was highly variable with poor imaging contrast, in lower expressing cells, PIKfyve could clearly be observed within both perinuclear clusters and in patches around macropinosomes (**Figure 1A**). Contrast was improved by expression in ΔPIKfyve cells, which completely rescued the swollen endosomal phenotype (**Figure S1A).** This allowed PIKfyve-GFP dynamics to be observed over time, demonstrating its recruitment to both macropinosomes and phagosomes within 60-seconds of engulfment (**Figure 1B** and **C, Movies 1 and 2**). Whilst low signal and movement in the Z-axis meant it was not possible to reliably follow individual macropinosomes much beyond ~2 minutes, we observed removal of PIKfyve-GFP from phagosomes approximately 3-minutes post engulfment. This confirms a role for PIKfyve in the early maturation of phagosomes and macropinosomes, consistent with its recruitment by PI(3)P and the defective initial acidification reported previously (Buckley et al., 2019).

Loss of PIKfyve specifically affects Rab7 delivery to phagosomes

To understand the functional role of PIKfyve, we examined how its loss affected other core components of the phagosome maturation pathway. In addition to PIPs, different stages of endosomal maturation are controlled by members of the Rab family of small GTPases. During classical endocytosis, Rab5 accumulates at early stages and exchanges with Rab7 as the vesicles mature (Rink et al., 2005). A similar Rab5-Rab7 exchange has been described during both phagosome and macropinosome maturation at around the same time we observe PIKfyve-GFP recruitment (Kerr et al., 2006; Poteryaev et al., 2010; Tu et al., 2022; Vieira et al., 2003).

Co-expression of RFP-Rab5a and GFP-Rab7A allowed us to follow the dynamics of both proteins to newly formed phagosomes in wildtype and ΔPIKfyve cells (**Figure 2A and B, Movie 3**). In wild-type cells, as previously reported (Tu et al., 2022), RFP-Rab5A was highly enriched on perinuclear endosomes, and to a lesser extent at the plasma membrane. We also observed that RFP-Rab5A became slightly enriched at phagocytic cups just prior to closure. This was independent of successful internalization (**Movie 4)**, suggesting a potential and

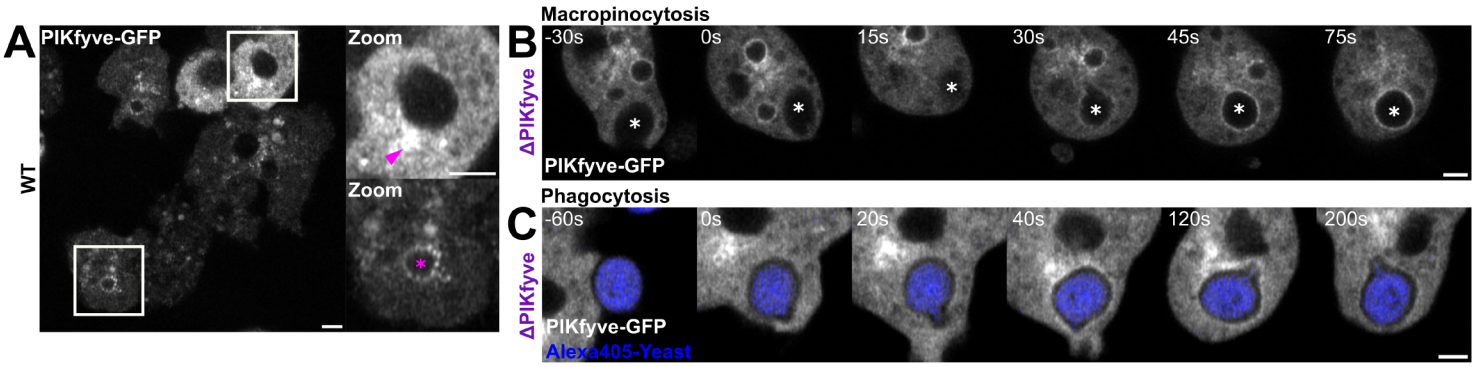

Figure 1: PIKfyve is enriched on early macropinosomes and phagosomes. (A) PIKfyve-GFP in wildtype *Dictyostelium* cells. PIKfyve is enriched on a peri-nuclear pool (pink arrow), and irregularly on the macropinosome membrane (pink star). (B) and (C) show PIKfyve-GFP localisation in *ΔPIKfyve* cells for increased contrast. Delivery to macropinosomes is shown in (B) with Alexa405-yeast containing phagosomes (blue) in (C). PIKfyve-GFP is delivered ~40 s post-formation and removed after 120 s. All scale bars = 2 μm.

unexplored role for Rab5 before engulfment is complete in *Dictyostelium*. RFP-Rab5A further intensified on phagosomes following internalization, peaking at around 1-minute post-engulfment before decreasing over the following minute. As expected, this coincided with a gradual accumulation with GFP-Rab7A, which localized to a large pool of small endosomes which continuously clustered around phagosomes and appeared to fuse from approximately 30 seconds post-engulfment. In ΔPIKfyve cells however, although RFP-Rab5A dynamics appeared identical, phagosomes never accumulated significant levels of GFP-Rab7A, despite its presence on other enlarged endocytic compartments (**Figure 2B**).

To quantify these differences, we developed an automated image analysis pipeline to measure the fluorescence intensity in a ring around the yeast over time and average over multiple events (**Figure S1B-D**). Acidification could also be measured from the signal from the pHrodo-labelled yeast (**Figure S1C**). To reduce the possibility of artefacts from overexpressing both proteins, Rabs were expressed individually as GFP-fusions (**Figure S2A-D** and **Movies 5 and 6)**. Although expression levels were somewhat lower in ΔPIKfyve cells (**Figure S2E**), this clearly demonstrated that loss of PIKfyve caused a specific defect in Rab7A accumulation on phagosomes while Rab5A dynamics were unperturbed (**Figure 2C and D**).

PIKfyve has multiple roles but is not important for Rab7 delivery to macropinosomes

To confirm normal Rab5 dynamics and activity, we also followed the dynamics of PI(3)P, which is generated by Rab5 activation of the Class II PI3-kinase VPS34 (Christoforidis et al., 1999). PI(3)P is also responsible for recruiting PIKfyve, and can followed using the well characterised reporter GFP-2xFYVE (Gillooly et al., 2000). Consistent with unperturbed Rab5, GFP-2xFYVE was recruited normally in ΔPIKfyve cells, becoming enriched on phagosomes within 60 seconds of engulfment (**Figure 2E-G, Movie 7**). Both GFP-2xFYVE and Rab7A were maintained on phagosomes for at least 50 minutes, most likely until the transition to a post-lysosome (**Figure S2F-H**) (Buczynski et al., 1997). Surprisingly, this differs from our previous observations of macropinosome maturation, where GFP-2xFYVE is removed ~5 minutes after formation (Buckley et al., 2019; King and Kay, 2019). The maturation of phagosomes and macropinosomes may therefore have important mechanistic differences.

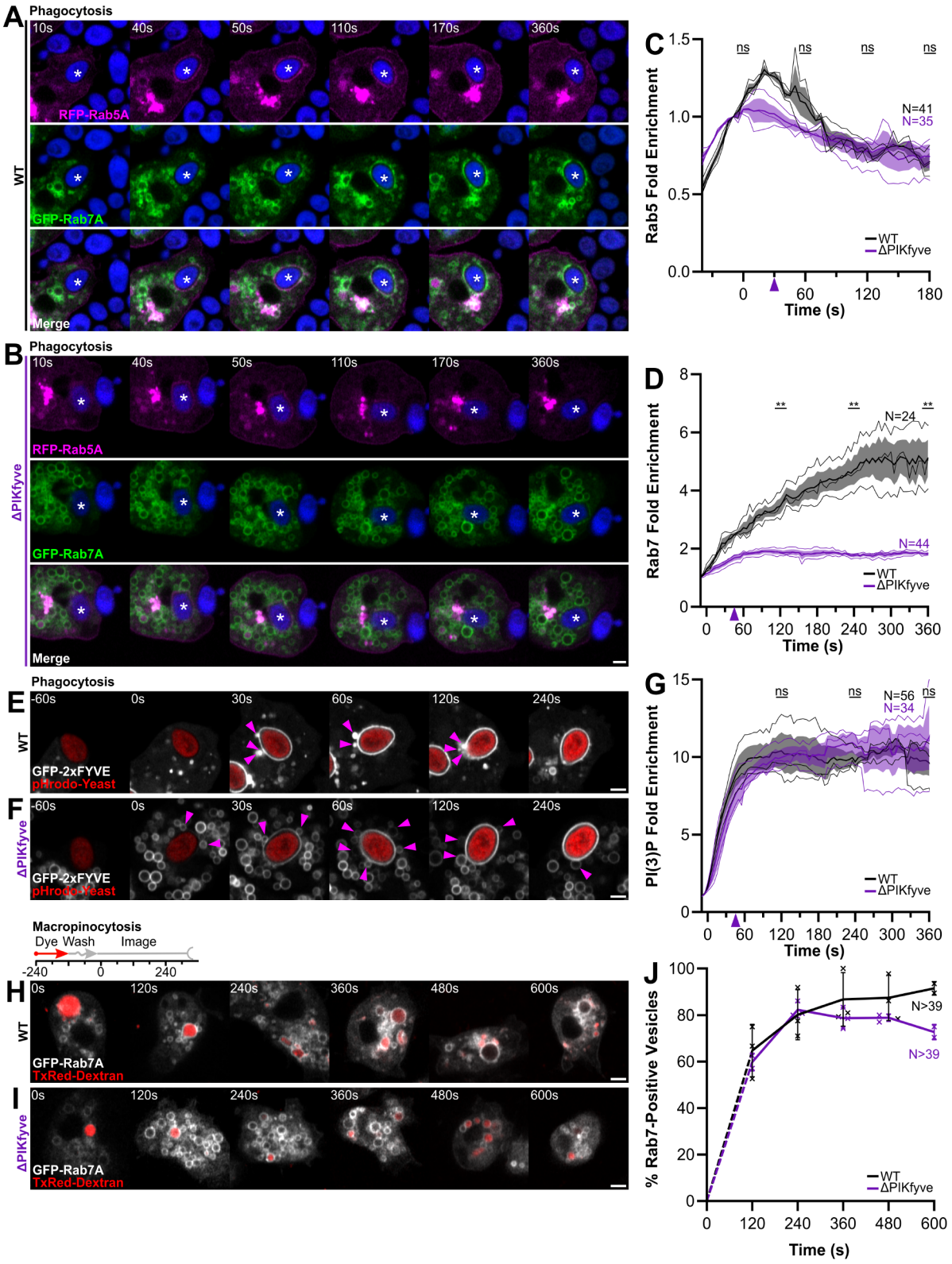

Figure 2: Loss of PIKfyve specifically affects Rab7 recruitment to phagosomes. Timelapse movies of (A) Wildtype and (B) *ΔPIKfyve* cells co-expressing RFP-Rab5A (magenta) and GFP-Rab7A (green) during phagocytosis of Alexa405-yeast (blue). The followed phagosome is indicted by and asterisk, see Movie 3 for full time series. RFP-Rab5A/GFP-Rab7A is clearly observed in wild-type cells, whilst ΔPIKfyve cells lose RFP-Rab5 normally, they fail to then accumulate GFP-Rab7A. Automated quantification of Rab5A and Rab7A recruitment to phagosomes is shown in (C) and (D) respectively, averaged over multiple movies when expressed individually as GFP-fusions. No significant differences in GFP-Rab5A enrichment were observed at any time point tested, but GFP-Rab7A was significantly decreased in ΔPIKfyve cells. (E) and (F) Representative timelapses of the PI(3)P reporter, GFP-2xFYVE, during phagocytosis of pHrodo-yeast (red) in wildtype and ΔPIKfyve cells. Pink arrows indicate GFP-2xFYVE labelled vesicles clustering around the phagosomal membrane from 30s. GFP-2xFYVE enrichment is quantified in (G). There were no statistically significant differences at any timepoints tested. (H) and (I) GFP-Rab7A recruitment to macropinosomes labelled by a 2 minute pulse of TxRed dextran (red) in wildtype and ΔPIKfyve cells. (J) Quantification by scoring the percentage of GFP-positive macropinosomes at each time point after dextran wash out. GFP-Rab7A dynamics are similar in both cell types. Data shown throughout are the mean ± SEM of 3 independent experiments, with N indicating the total number of cells measured. The means of each independent repeat are indicated by the additional thin lines in C,D and J and the crosses in J. Statistical significances in C, D and J were calculated by unpaired T-test of a 5-point rolling average. The purple arrow on each graph indicates the time of GFP-PIKfyve arrival. All scale bars =

Although GFP-Rab7A did not accumulate on ΔPIKfyve phagosomes, it clearly still localised to other large endocytic compartments (**Figure 2B**). As these resemble the swollen macropinosomes previously observed in these cells (Buckley et al., 2019), we asked whether the defect in GFP-Rab7A delivery was specific to phagosome maturation. As individual macropinosomes are difficult to follow for more than 2-3 minutes by timelapse microscopy, we labelled macropinosomes with a 2-minute pulse of TexasRed-dextran. Different fields of view were then captured at time intervals after dextran removal allowing the percentage of macropinosomes positive for GFP to be measured for up to 10 minutes (Buckley et al., 2016). In this assay, GFP-Rab7A recruitment to macropinosomes was indistinguishable between ΔPIKfyve cells and wild-type controls, accumulating within 2 minutes of internalisation (**Figure 2H-J)**. PIKfyve is therefore specifically important for the accumulation of Rab7 on phagosomes, but not macropinosomes.

However, despite having normal Rab7A dynamics, the macropinosomes in ΔPIKfyve cells appeared to be much larger. Quantification of the size and fluorescence intensity of these demonstrated that although macropinosomes started off the same size in both cell lines, the normal shrinkage and concentation of their lumen observed in wild-type controls was significantly impaired in *PIKfyve* mutants (**Figure S2I)**. To functionally test whether macropinosome digestion proceeds normally, we measured proteolysis of fluid-phase DQ-BSA by flow cytometry. Whilst loss of PIKfyve almost completely blocks proteolysis of this dye conjugated to beads (Buckley et al., 2019), digestion of the fluid-phase dye occurs normally (**Figure S2J**). Therefore, PIKfyve plays an additional role during macropinosome shrinkage, independent from Rab7 delivery and digestion, which is only affected during phagosome maturation.

Identification of a novel, reliable PI(3,5)P2 reporter

A current major limitation of all studies of PIKfyve and PI(3,5)P2 is the lack of a reliable reporter to show where and when the lipid is generated. Although a probe based on tandem repeats of the N-terminal domain of mucolipin1 (GFP-ML1N) shows good specificity for PI(3,5)P2 *in vitro*, it has poor selectivity within cells (Dong et al., 2010; Hammond et al., 2015; Samie et al., 2013). We therefore sought to identify novel PI(3,5)P2 binding proteins in *Dictyostelium*.

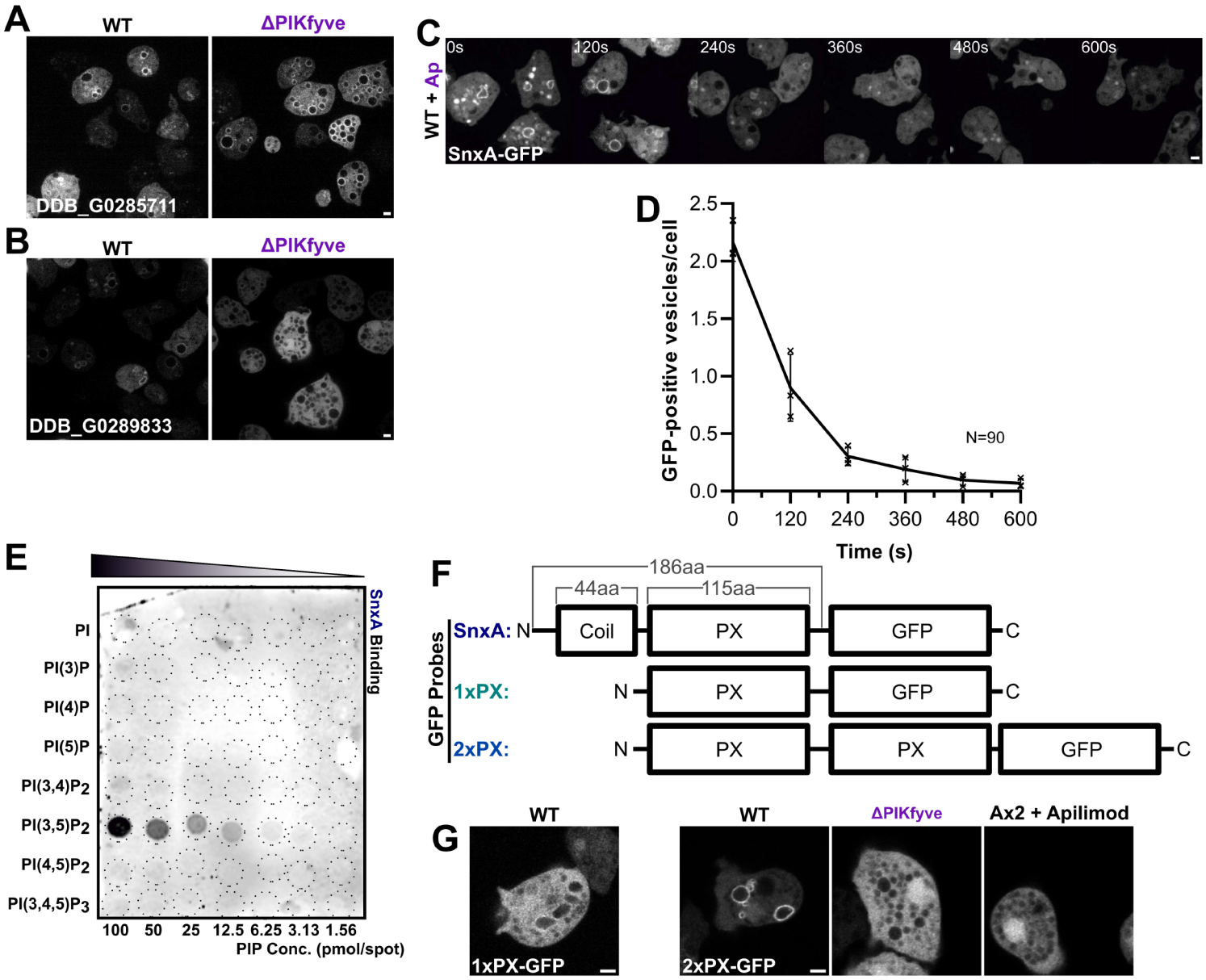

Figure 3: Identification of SnxA as a PI(3,5)P2 reporter. (A) and (B) Expression of GFP-fusions of PX-domain containing proteins in wildtype and ΔPIKfyve Ax3 Dictyostelium. (A) DDB_G0285711 localised to large vesicles in both cells, whereas DDB_G0289833 (B) was completely cytosolic in ΔPIKfyve. (C) Timelapse of DDB_G0289833 (Snx-A)-GFP localistion in Ax2 cells after addition of the PIKfyve inhibitor apilimod (3 μM). Quantification of number of SnxA-GFP vesicles per cell is shown in (D). >90 cells measured per time-point. Data shows mean ± SEM of 3 independent experiments. (E) PIP array using lysates from wildtype cells expressing SnxA-GFP and probed with anti-GFP antibody. (F) Schematics of SnxA-GFP, 1xPX-GFP and 2xPX-GFP. (G) Representative images of their localisation in the cells indicated. 1xPX-GFP remained predominately cytosolic in wildtype cells, whereas 2xPX-GFP localised strongly to large vesicles, which was lost in ΔPIKfyve and apilimod treated cells. All scale bars = 2 μm.

We hypothesised that *Dictyostelium* must have specific PI(3,5)P2-binding proteins that are only recruited in the presence of PIKfyve. PX-domains are frequently used by proteins to bind specific PIPs. We therefore screened C-terminally tagged GFP fusions of *Dictyostelium* PX-domain containing proteins for PIKfyve-dependent localization, by expression in both wild-type and ΔPIKfyve cells.

Of the proteins cloned, most localised to membranes irrespective of the presence or absence of PIKfyve (e.g. **Figure 3A**). However, one (DDB_G0289833) clearly localised to large vesicles with the appearance of macropinosomes in wildtype, but was completely cytosolic in ΔPIKfyve cells (**Figure 3B)**. DDB_G0289833 is previously unstudied and contains a coiled-coil domain in addition to the PX-domain. As this domain combination is found in many mammalian sorting nexins we therefore named the *Dictyostelium* protein SnxA. To further confirm the dependence of SnxA recruitment on PIKfyve we applied the PIKfyve inhibitor apilimod (Cai et al., 2013) to wildtype cells expressing SnxA-GFP. This caused rapid dissociation of SnxA-GFP from all membranes, becoming completely cytosolic within 10 minutes (**Figure 3C-D**).

PIKfyve activity is required for the formation of both PI(3,5)P2 and PI(5)P. To determine the lipid-binding specificity of SnxA we examined binding to PIP arrays using lysates from SnxA-GFP expressing *Dictyostelium* cells. In this assay SnxA-GFP bound with at least a 20-fold preference to PI(3,5)P2 over all other PIPs with almost no non-specific binding at even the highest lipid concentrations (**Figure 3E**).

To optimise lipid binding and reporter characteristics, we then tested GFP-fusions of either the PX-domain alone, or a tandem repeat of this domain (1xPX and 2xPX-GFP respectively, **Figure 3F**). 1xPX-GFP had low contrast, localising poorly to large vesicles in some cells but was completely cytosolic in many others. Contrast was significantly enhanced in the 2xPX construct, which localised with similar characteristics and PIKfyve-dependence as full-length SnxA-GFP (**Figure 3G**). The 2xPX-GFP construct also bound similarly to PIP arrays, localizing specifically to PI(3,5)P2 (**Figure S3A**).

To confirm PI(3,5)P2- specificity to more physiologically-relevant membranes, all three GFP fusions were produced recombinantly (**Figure S3B**) and screened for binding to beads coated with bilayers consisting of 5% phosphoinositide and 95% POPC. Lipid binding and affinities

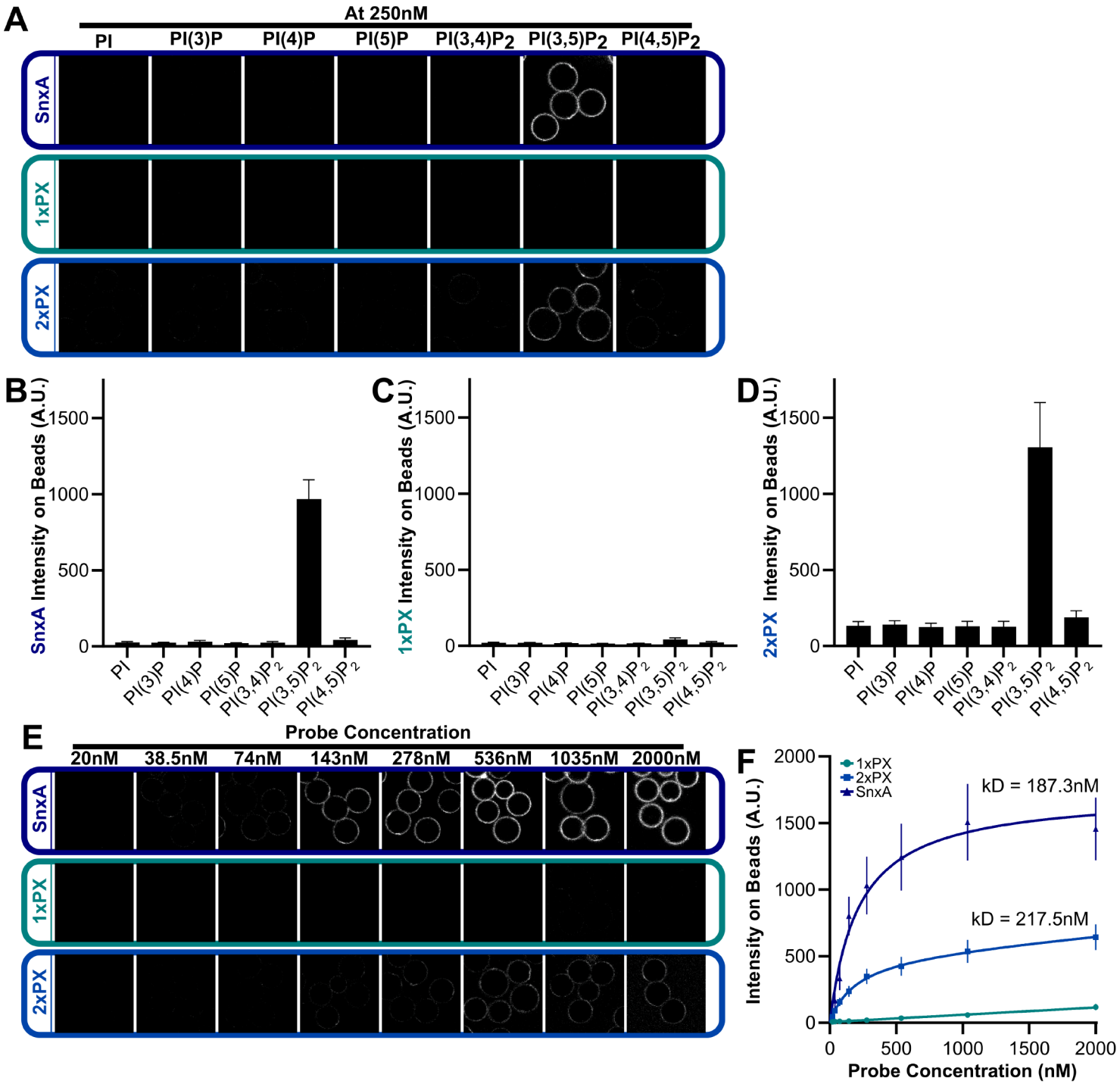

Figure 4: PI(3,5)P2 binding specificity of SnxA. (A-D) Representative images and quantification of recombinant GFP-SnxA probes to membrane coated beads containing the indicated PIPs. (E) Binding of each SnxA probe titrated against beads harboring PI(3,5)P2. Intensities and apparent K_ds are shown in (F). All graphs show the mean ± standard deviation from 3 independent experiments.

were then determined by measuring GFP recruitment by microscopy (Maib and Murray, 2022). As anticipated, both SnxA-GFP and 2xPX-GFP probes showed high specificity for PI(3,5)P2, while 1xPX showed very little binding (**Figure 4A-D**). By titrating the probe concentration at a fixed amount of membrane, we determined an apparent Kd of 187.3nM for full-length SnxA and 217.5nM for 2xPX (**Figure 4E-F**). Importantly, no binding to PI(5)P, the other product of PIKfyve, was observed under any conditions (**Figure S3C and D**).

These data demonstrate that the PX domain of SnxA is a highly selective PI(3,5)P2-binding domain. Whilst a tandem repeat of this domain increases binding affinity, this provides no improvement over the full-length protein. We speculate that this is due to dimerization of the full-length protein through the coiled-coil region, which is also advantageous as it will incorporate 2 GFP-moieties in each dimer. Rapid dissociation *in vivo* upon PIKfyve inhibition also demonstrates fast off-kinetics, indicating that SnxA-GFP can be reliably used to indicate PI(3,5)P2 dynamics and localisation in live cells. For optimal imaging and uniform expression levels we then generated a stably integrated SnxA-GFP cell line selecting for a clone with low expression/high contrast for microscopy experiments.

SnxA is not important for phagosome or macropinosome maturation

As SnxA specifically binds PI(3,5)P2 downstream of PIKfyve, we generated multiple independent *SnxA* knockouts and asked whether it played an important function in phagosome maturation itself. However, unlike ΔPIKfyve cells, ΔSnxA mutants had no significant defects in growth on bacteria, bulk fluid uptake, phagocytosis, phagosome proteolysis or acidification (**Figure S4A-G**).

Despite extensive investigation, the only differences we could observe between wild-type and ΔSnxA cells was a subtle but reproducible alteration in the dynamics of macropinosome shrinkage after internalisation: whilst wild-type macropinosomes transiently enlarge after internalisation before shrinking and concentrating, the expansion phase does not occur in ΔSnxA cells and can be rescued by re-expression of SnxA-GFP (**Figure S4H-I**). Despite this, bulk fluid uptake is unaffected and no axenic growth defect was observed. We speculate the transient swelling indicates SnxA-dependent fusion of another endocytic compartment to very early macropinosomes, but this requires further investigation. In any case, SnxA is not necessary for maturation of either phagosomes or macropinosomes.

PI(3,5)P2 dynamics during macropinosome and phagosome maturation

Next, we used the SnxA-GFP reporter to characterise PI(3,5)P2 dynamics for the first time. To observe SnxA-GFP recruitment to phagosomes, we used timelapse confocal microscopy of cells engulfing pHrodo labelled yeast. This showed phagosomes acquire a burst of PI(3,5)P2 2 minutes after engulfment, which was retained for at least 30 minutes (**Figure 5A-C, S6A** and **Movie 8**). SnxA-GFP was completely absent from phagosomal membranes in ΔPIKfyve cells, remaining entirely cytosolic.

Surprisingly, phagosomal accumulation of PI(3,5)P2 on appeared to be accompanied by the docking and fusion of multiple smaller SnxA-GFP-positive vesicles. These cluster and dock several seconds before the phagosomal membrane itself acquires the reporter arrows in **Figure 5A**). This implies that PI(3,5)P2 can accumulate through both *in situ* synthesis by PIKfyve and delivery via fusion with another PI(3,5)P2 compartment.

Timelapse imaging of SnxA-GFP recruitment to macropinosomes indicated that PI(3,5)P2 accumulated with a similar timing and vesicle clustering as phagosomes (**Figure 5D)**. To follow macropinosomes for a longer time, we again labelled them with a 2 minute dextran pulse and followed colocalization with SnxA-GFP over time. This confirmed SnxA-GFP recruitment within the first minutes after engulfment, peaking at 4 minutes - slightly slower than PI(3)P, which arrives at the earliest observable time point with this method (**Figure 5E and F**). Unlike phagosomes, SnxA-GFP was lost from macropinosomes after 5-6 minutes.

To confirm the relative dynamics of PI(3)P and PI(3,5)P2, we co-expressed SnxA-GFP with RFP-2xFYVE. Although RFP-2xFYVE expression slowed maturation dynamics, it was recruited to both macropinosomes and phagosome immediately following internalisation, with SnxA-GFP arriving several minutes later (**Figure S5C and D** and **Movie 9**).

PIKfyve activity and recruitment are highly regulated

Both macropinosomes and phagosomes accumulate PI(3,5)P2 abruptly 90-120s after internalisation. However, both PIKfyve and its substrate PI(3)P accumulate almost a minute earlier (**Figure 1** and **2D**), indicating an additional regulatory step for PI(3,5)P2 accumulation.

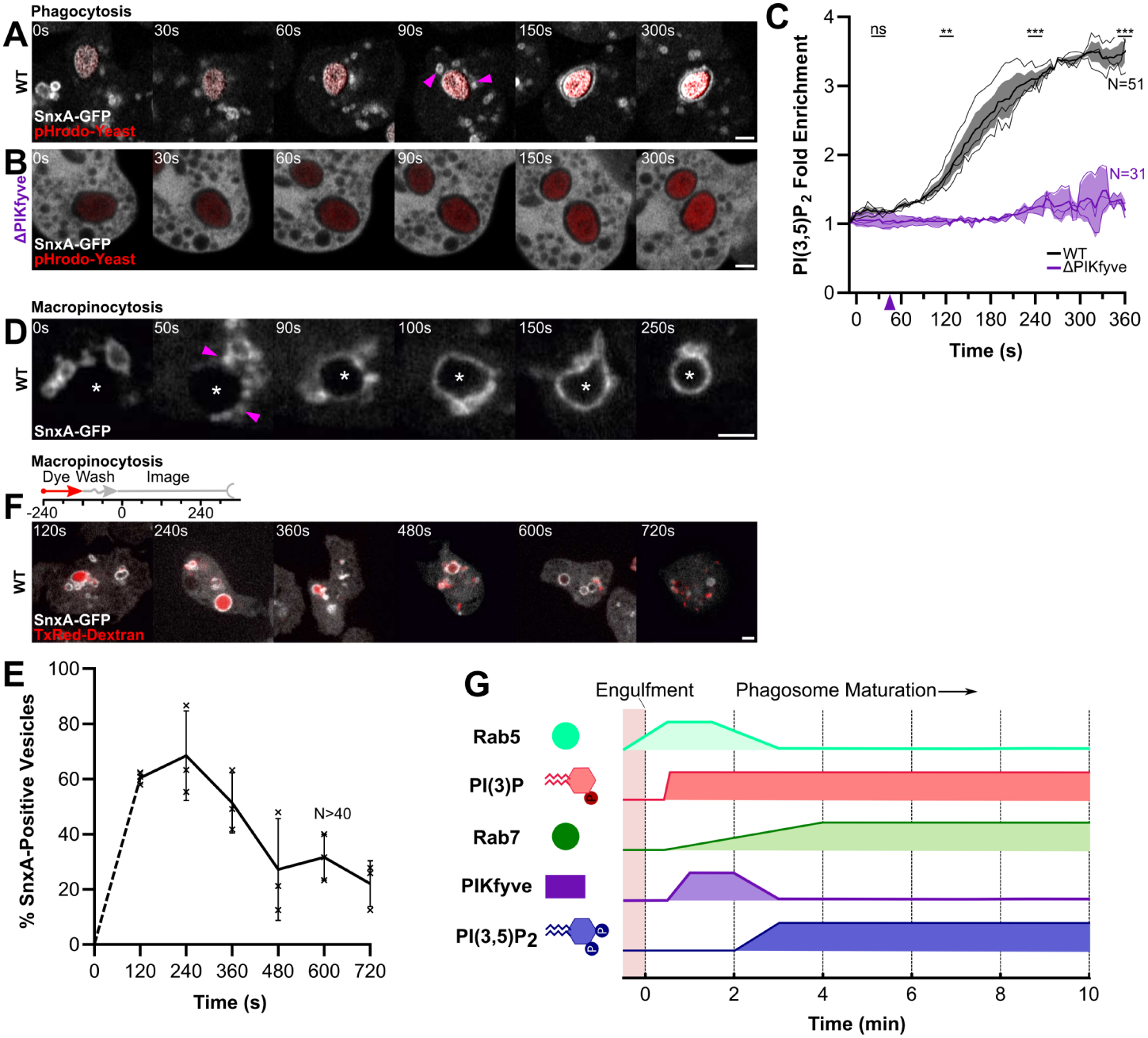

Figure 5: PI(3,5)P2 dynamics during macropinosome and phagosome maturation. (A) and (B) Timelapses of SnxA-GFP during phagocytosis of pHrodo-yeast (red) in wildtype (A) and ΔPIKfyve (B) cells. Pink arrowheads indicates clustering SnxA vesicles. (C) Quantification of SnxA-GFP enrichment at the phagosomal membrane for 51 wildtype and 31 ΔPIKfyve phagosomes across 3 independent experiments. Fold enrichment normalised to 10 s before engulfment. Purple arrow indicates time of PIKfyve arrival from Figure 1. (D) Timelapse of SnxA-GFP recruitment to a newly formed macropinosome (marked by asterisk). Pink arrowheads indicate clustered vesicles prior to fusion. (E) Longer-term imaging of SnxA-GFP recruitment to macropinosomes via a 2 minute dextran pulse-chase. Different fields of view were taken at time points after dextran wash-out. The proportion of SnxA-GFP positive macropinosomes at each time after dextran addition is shown in (F). >40 vesicles were counted per time-point across 3 independent experiments. Both graphs show the mean ± SEM of 3 independent experiments. All scale bars = 2 μm. (G) Schematic summary of the dynamics of each component studied on the phagosomal membrane.

To investigate the correlation between PIKfyve recruitment and PI(3,5)P2 accumulation, we co-expressed GFP-PIKfyve with the SnxA probe (2xPX) in cells engulfing alexa-405 labelled yeast. This confirmed that PIKfyve is recruited 1-2 minutes prior to PI(3,5)P2 accumulation but also showed that they only co-localise fleetingly, with PIKfyve-GFP dissociating immediately after the SnxA probe arrives (**Figure 6A and B** and **Movie 10**). This indicates a mechanism whereby PIKfyve is recruited early, but only becomes active later in a burst which couples PI(3,5)P2 accumulation and its own dissociation. As PIKfyve is constitutively in a complex with the phosphatase FIG4, which could break down PI(3,5)P2 (Bonangelino et al., 2002), we speculate removal of the complex may be necessary to maintain PI(3,5)P2 levels on the phagosomal membrane.

To test whether PIKfyve activity is required for its release from phagosomes, we treated cells expressing PIKfyve-GFP with its inhibitor apilimod. As predicted, apilimod-treated cells accumulated PIKfyve-GFP more strongly than untreated cells, and timelapse microscopy showed that inhibited PIKfyve was retained on phagosomes significantly longer (**Figure 6C-F**). As PI(3)P is present throughout (**Figure 2F**), this demonstrates that recruitment of PIKfyve via its FYVE-domain is regulated by its catalytic activity, providing a mechanism to couple activity and release.

PI(3,5)P2 is delivered by fusion of small Rab7 and PI(3)P positive vesicles

Although PIKfyve-GFP is only present on nascent phagosomes and macropinosomes, during timelapse experiments we noticed SnxA-GFP appears to accumulate via the docking and delivery of small SnxA-positive vesicles (arrows in **Figure 5A and F**, **Movies 8 and 9**). These vesicles cluster around phagosomes and macropinosomes from 60-seconds post engulfment, and appear to fuse at the point the phagosome/macropinosome accumulates the SnxA-GFP probe and PIKfyve dissociates. Therefore, PI(3,5)P2 appears to be delivered by vesicle fusion in addition to local synthesis by phosphorylation of PI(3)P. This mechanism of delivery would imply that PIKfyve activity may coordinate homotypic fusion between PI(3,5)P2 containing compartments.

To determine the identity of the PI(3,5)P2-containing vesicles that fuse with early phagosomes and macropinosomes we co-expressed SnxA-GFP with RFP-fusions of Rab7A or the VatM component of the V-ATPase. Timelapse microscopy of both phagosomes and macropinosomes indicated that all docked SnxA-positive vesicles were also both Rab7A and

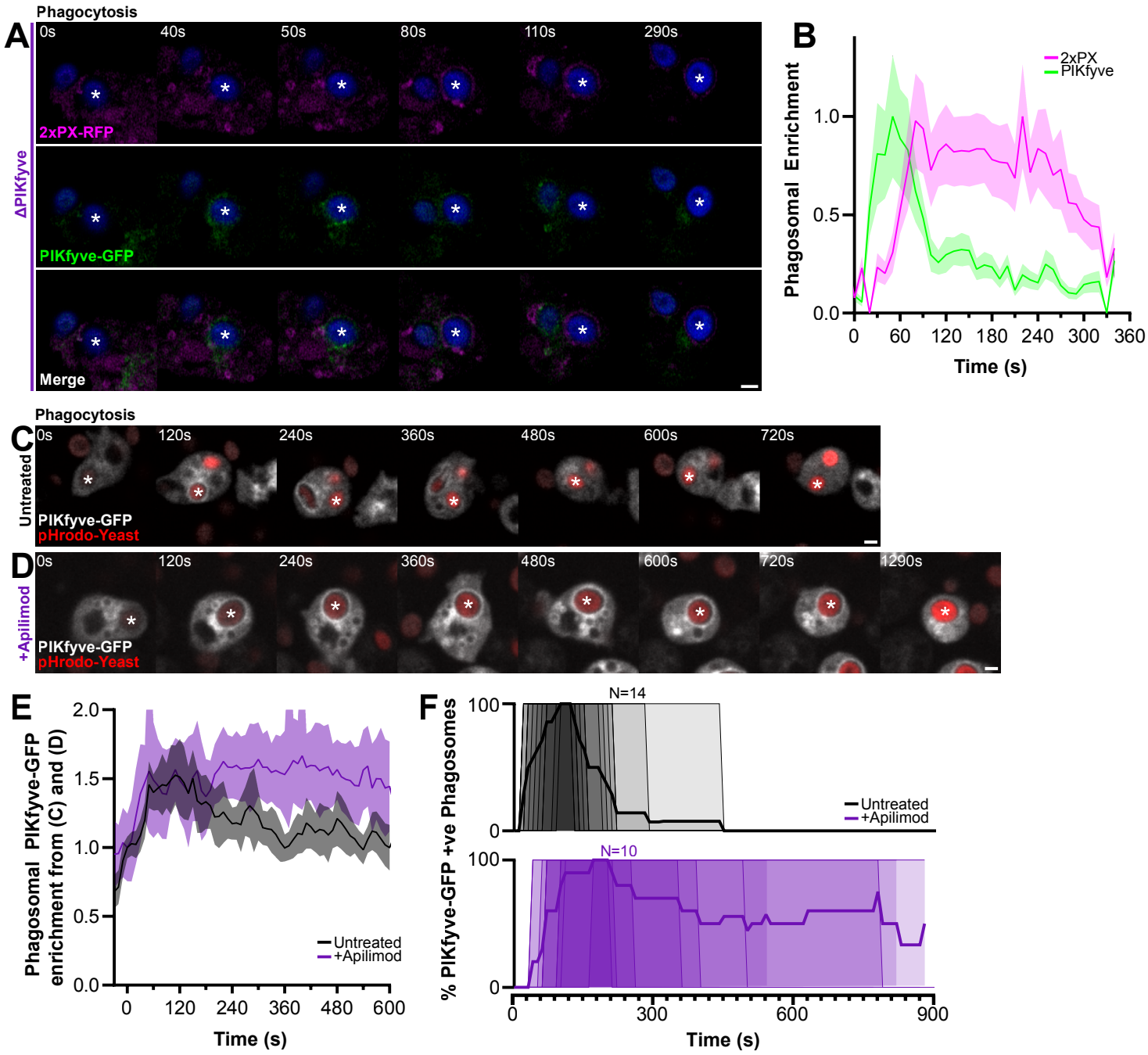

Figure 6: Regulation of PIKfyve activity and recruitment. (A) Timelapse of cells coexpressing 2xPX-RFP (magenta) and PIKfyve-GFP (green) during phagocytosis of Alexa405-yeast (blue). (B) Fluorescence intensity around the phagosome in (A). Data shown is the mean intensity ± the standard deviation around the phagosomal membrane normalised between minimum and maximum intensities observed. (C) and (D) Timelapse of PIKfyve-GFP during phagocytosis of pHrodo-yeast (red) in cells before (C) and after (D) addition of 5μM apilimod. The PIKfyve-GFP intensity around the phagosome in these movies is quantified in (E). (F) Shows the PIKfyve-GFP dynamics over multiple events, by manually scoring the time of PIKfyve-GFP delivery and release. 14 untreated events and 10 apilimod treated events were scored and the thick line indicates the proportion of GFP-positive phagosomes at each time after engulfment. Thin lines represent individual events. All scale bars = 2 μm.

V-ATPase positive (**Figure 7A and B and Figure S6A**). However, both Rab7A and VatM also localised to additional populations of vesicles that start to cluster and fuse much earlier than those marked by SnxA, from ~20 seconds post-internalisation (**Figure 7C-D** and **Figure S6A**).

These findings show that multiple different populations of vesicles fuse with phagosomes and macropinosomes over the first few minutes of maturation. These include a very early population marked by PI(3)P, Rab7 and the V-ATPase which begin to fuse within the first minute of maturation, as well as later PI(3,5)P2 compartments which fuse synchronously about a minute later, at the point PIKfyve dissociates.

PIKfyve is required for the delivery of early macropinosomes to phagosomes

As loss of PI(3,5)P2/Rab7 delivery would explain the defective Rab7 accumulation and maturation observed in ΔPIKfyve cells, we sought to identify the origin of these PI(3,5)P2/Rab7 positive vesicles. We observed above that early macropinosomes are marked by both these components (**Figure 5D-E**), and others have shown that macropinosomes undergo homotypic fusion in both *Dictyostelium* and mammalian cells (Dolat and Spiliotis, 2016; Hamasaki et al., 2004; Neuhaus et al., 2002; Tu et al., 2022). Using sequential pulses of different coloured dextrans, we were also able to observe macropinosomes fusing with one another from relatively early stages of maturation (**Figure S6B**). Therefore, we hypothesized that macropinosomes and phagosomes fuse in a PIKfyve-dependent manner.

To test this, we labelled macropinosomes by incubating cells with a 70kDa dextran for 5 minutes, before washing and addition of yeast. In this way we were able to follow interactions between a defined population of dextran-filled macropinosomes and nascent phagosomes. In wildtype cells, small numbers of macropinosomes began clustering around phagosomes within 30-seconds of engulfment, becoming gradually more prominent by 60-seconds (**Figure 8A**). At this point these macropinosomes must be between 3 and 8 minutes old, including the 2 minutes taken during washing. Quantification of the average dextran signal within 0.5 µm of the yeast showed that macropinosomes remained clustered around phagosomes for several minutes, as we previously observed for GFP-Rab7A. Macropinosome clustering was completely lost in ΔPIKfyve cells, where the enlarged macropinosomes were never clearly observed interacting with the phagosome (**Figure 8B and C**).

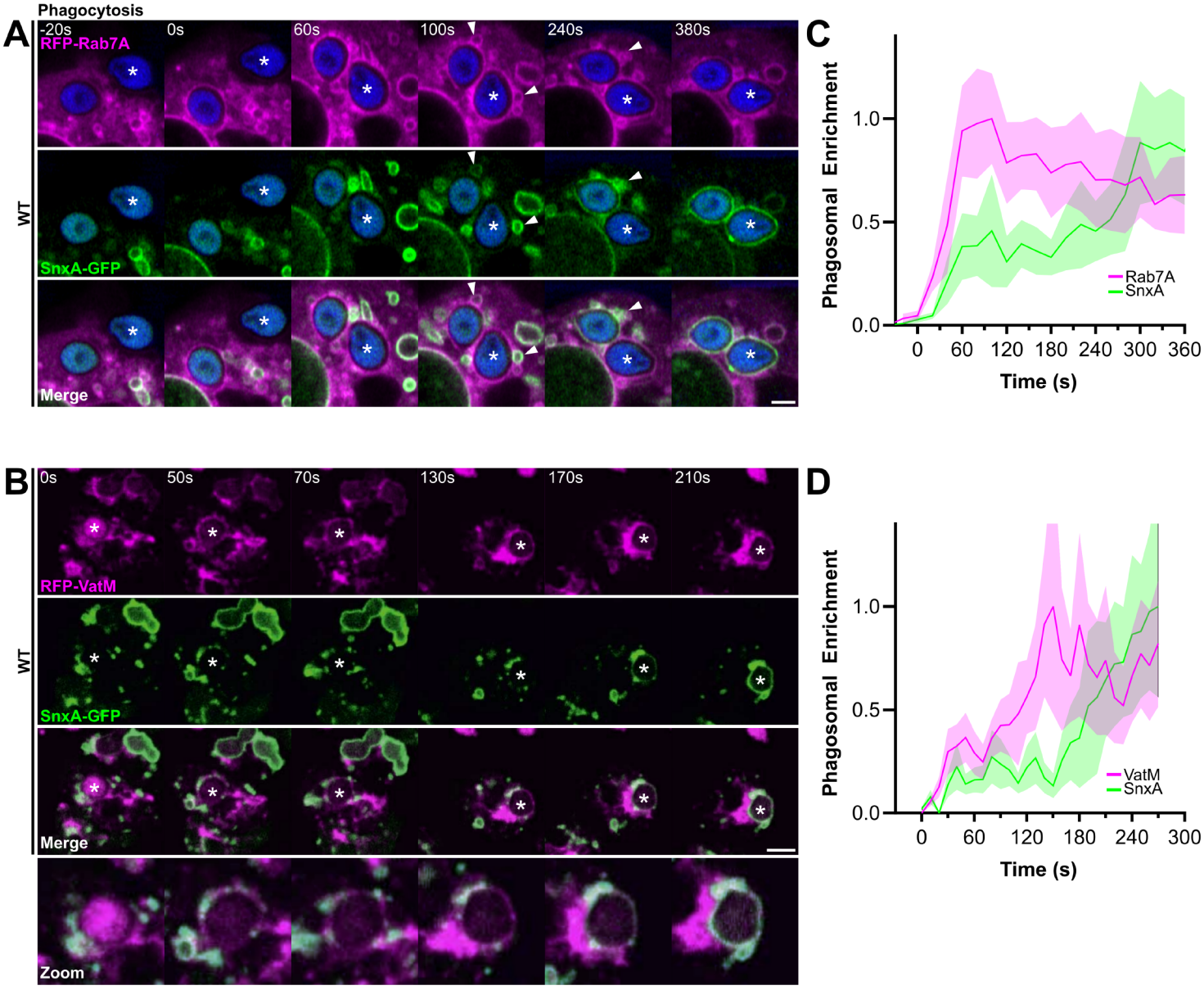

Figure 7: SnxA is delivered after Rab7 and VatM. (A) Timelapses of RFP-Rab7A (magenta) and SnxA-GFP (green) during phagocytosis of Alexa405-yeast (blue) in wildtype cells. SnxA and Rab7 co-localize on many clustering vesicles (arrowheads) (B) Timelapse of VatM-RFP (magenta) and SnxA-GFP (green) during phagocytosis of Alexa405-yeast (blue). Fluorescence intensity around phagosomes in A and B, are shown in (C) and (D) respectively. Data is mean intensity ± SD of a linescan along the phagosomal membrane normalised between minimum and maximum intensities observed.

To determine whether macropinosomes were just clustering around phagosomes or fusing with them, we also examined delivery of dextran to the phagosomal lumen. Using GFP-2xFYVE to highlight the bounding phagosomal membrane, it was occasionally possible to observe dextran accumulation in small pockets that appeared to be within the phagosomal envelope (**Figure 8D**). This was difficult to reliably quantify, but we noticed that when budding yeast were used, dextran accumulated prominently within the bud neck region of the phagosome due to its negative curvature (**Figure 8E)**. Using budded yeast therefore enabled us to reproducibly observe and quantify dextran delivery within the phagosome. This demonstrated fusion of early macropinosomes to phagosomes in wild-type cells, that was completely lost in ΔPIKfyve cells (**Figure 8F**). Therefore, PIKfyve is required for both clustering and delivery of macropinosomes to early phagosomes.

To determine whether the clustering macropinosomes were the same PI(3,5)P2/PI(3)P/Rab7 populations observed above (**Figures 2 and 7**), we imaged macropinosome clustering in cells expressing each GFP-fusion reporter. At 2-minute intervals post-phagocytosis, all macropinosomes within 1 μm of the phagosomal membrane were then scored for colocalization of each reporter (**Figure 8G-I**).

In each experiment, the number of docked macropinosomes started low (initially ~2 per phagosome) but increased to ~6 per phagosome by 2 minutes. Over 80% of these were positive for GFP-Rab7A throughout the experiment, whilst the proportion positive for PI(3)P started high, but fell over time. This is consistent with PI(3)P arrival on phagosomes, and points to a population of PI(3)P and Rab7-positive macropinosomes which dock at the very early stages of phagosome maturation. In contrast, the percentage of SnxA-GFP positive macropinosomes at the phagosome started low, but increased so that ~80% of docked macropinosomes were SnxA-GFP positive at 6-8 minutes. This result is again consistent with our timelapses of SnxA delivery, and demonstrates that the majority, if not all, the PI(3,5)P2-positive vesicles that fuses with early phagosomes are early macropinosomes.

As both PI(3)P and PI(3,5)P2 are only present on macropinosomes for the first 7-8 minutes of maturation (**Figure 5E and F**), we asked if only early macropinosomes were fusion competent over this period. To test this, cells were again exposed to a 5-minute pulse of dextran, but were then incubated for these macropinosomes to mature for 10 minutes before

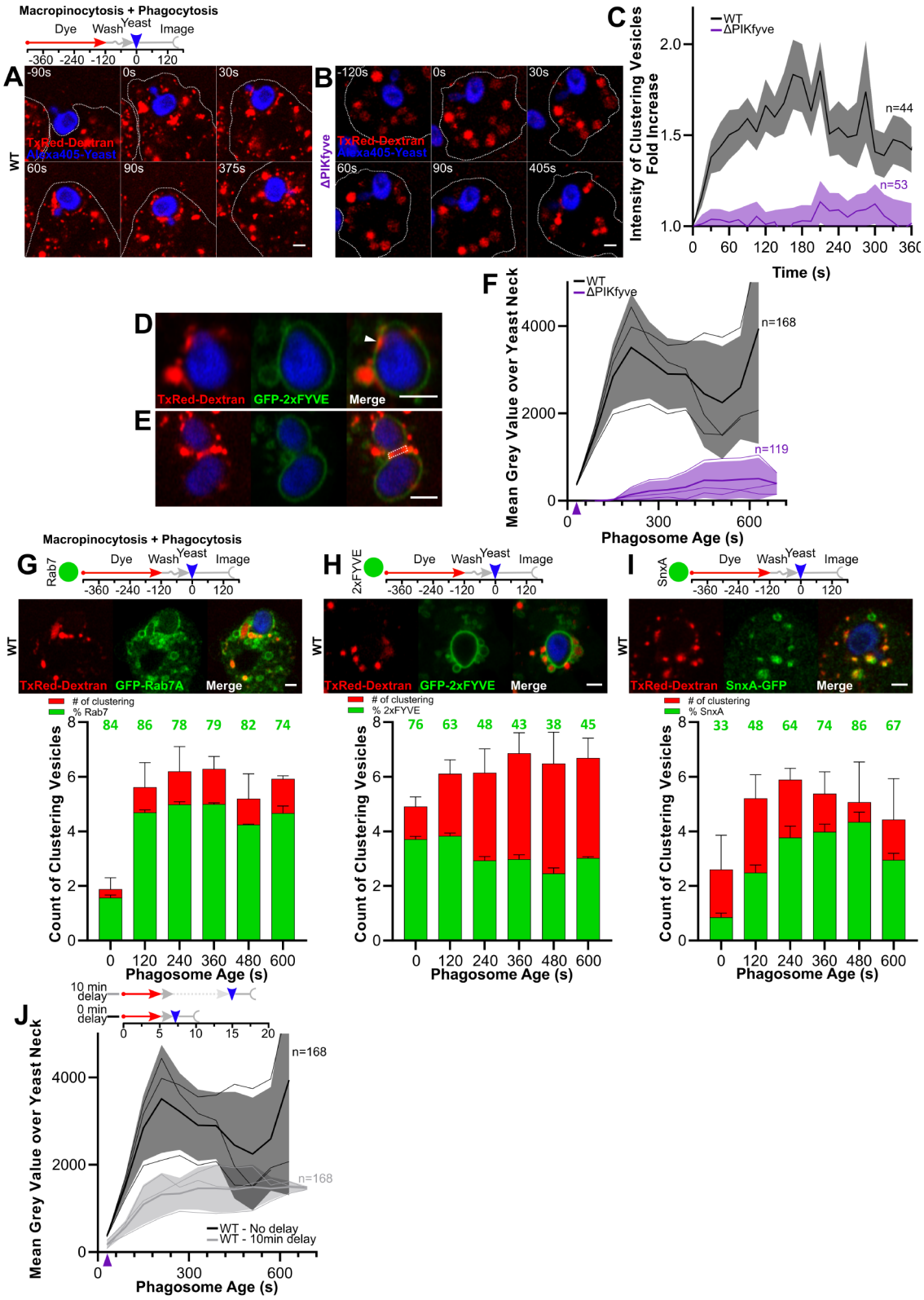

Figure 8: PIKfyve drives fusion between macropinosomes and phagosomes. (A) and (B) Timelapses of interactions between early (<5mins) macropinosomes (red) and phagosomes (blue) in wildtype and ΔPIKfyve cells, after sequential addition of fluorescent dextran and yeast. Schematic shows experimental procedure. Macropinosomes cluster around phagosomes in wildtype but not in ΔPIKfyve cells. (C) Quantification of dextran intensity around phagosomes, averaged over multiple events. Graph shows fold enrichment normalised to 10s before engulfment ± SEM. (D) TxRed-dextran (red) accumulation within the phagosomal membrane (green) marked by 2xFYVE (arrowhead). (E) Shows the same, using a budded yeast. Note strong dextran accumulation around the bud neck (dashed box). (F) Quantification of dextran intensity in this area averaged across multiple events ± SEM, binned by the age of the phagosome. (G-I) Images and quantification of clustering macropinosome identity. Wildtype cells expressing GFP-Rab7A, GFP-2xFYVE or SnxA-GFP were treated with a dextran pulse-chase before phagocytosis of yeast. Macropinosomes within 1 µm of the phagosome were identified at each timepoint and both total number (red bars) and proportion colocalizing with the respective GFP-reporter (green bars and numbers) were scored manually. Frames were binned into 2- minute groups, data shown are the mean ±SEM of three independent experiments. Note increased clustering from 2 minutes, with high Rab7 colocalization, followed by an increase in SnxA-GFP positive macropinosomes after 4 mins. (J) Quantification of dextran delivery (as in F) after a 10-minute delay before addition of yeast (see schematic, same control data as in F). Older macropinosomes show less delivery to phagosomes. All purple arrows on graphs indicate the time of PIKfyve arrival. All scale bars = 2 µm.

yeast addition. In both cases dextran accumulation at the yeast neck was significantly decreased (**Figure 8J**). This was less reduced than that observed in ΔPIKfyve cells with ~20% of the dextran delivery remaining, which can potentially be attributed to older macropinosomes fusing to newer macropinosomes which are then able to fuse. Macropinosomes are therefore only competent to fuse with phagosomes at a specific early stage (2-8 minutes old), when they posess both PI(3)P and PI(3,5)P2.

Our data demonstrate a specific role for PIKfyve in the delivery of macropinosomes to newly formed phagosomes, in addition to mechanistic insights into the dynamics and regulation of PI(3,5)P2 synthesis. As these macropinosomes are enriched in V-ATPase, Rab7 and lysosomal enzymes, this provides a mechanism for their rapid delivery to early phagosomes, which is physiologically important for effective bacterial killing and protection from pathogens (Buckley et al., 2019).

Discussion

In this study we expand our understanding of the complex dynamics of Rab and phosphoinositide signalling that underpin the processing of phagosomes and macropinosomes. We describe a complex pathway, where multiple different pools of vesicles are delivered at different times over the first few minutes of maturation and define a key regulatory role for PIKfyve and its product PI(3,5)P2. The inability to observe PI(3,5)P2 dynamics in live cells has been a major limitation within the field. By identifying the *Dictyostelium* protein SnxA as a faithful PI(3,5)P2 reporter, we have been able to unpick the complex regulation of PIKfyve and its effects on trafficking for the first time.

Our observations of the localisation and dynamics of both the PIKfyve enzyme and its product provide several new mechanistic insights. Combined, our data support a model whereby PIKfyve is regulated in a series of coordinated steps: (1) inactive PIKfyve is recruited by binding PI(3)P, (2) acute activation of PIKfyve and PI(3,5)P2 accumulation, (3) fusion of additional PI(3,5)P2- containing vesicles, (4) PIKfyve dissociation, dependent on its own activity (**Figure 9**).

Complex regulation is not unexpected. PIKfyve is unusual in that its catalytic substrate (PI(3)P) also mediates its recruitment via additional interactions with the FYVE domain. Whilst PIKfyve could be released from the membrane by simply using up all the PI(3)P (Kerr et al., 2010), this cannot be the case in this system as PI(3)P is retained on phagosomes long after PIKfyve dissociates and loss of PIKfyve does not affect PI(3)P dynamics (**Figure 2** and (Buckley et al., 2019)). There must therefore be additional regulation of the FYVE domain binding. This is consistent with a recent study demonstrating recruitment of the yeast PIKfyve orthologue Fab1 is regulated by phosphorylation near its FYVE domain by TORC1, causing translocation between the yeast vacuole and signalling endosomes (Chen et al., 2021). Whilst it is unclear whether this mechanism is conserved in other endocytic pathways or organisms, PIKfyve recruitment to PI(3)P must also be conditionally regulated during *Dictyostelium* phagosome maturation.

A further complication is that PIKfyve is complexed with the phosphatase Fig4 which can potentially break down PI(3,5)P2 as soon as it is generated. As PI(3,5)P2 accumulates in a burst almost 2 minutes after PIKfyve arrival, either PIKfyve or Fig4 catalytic activity must

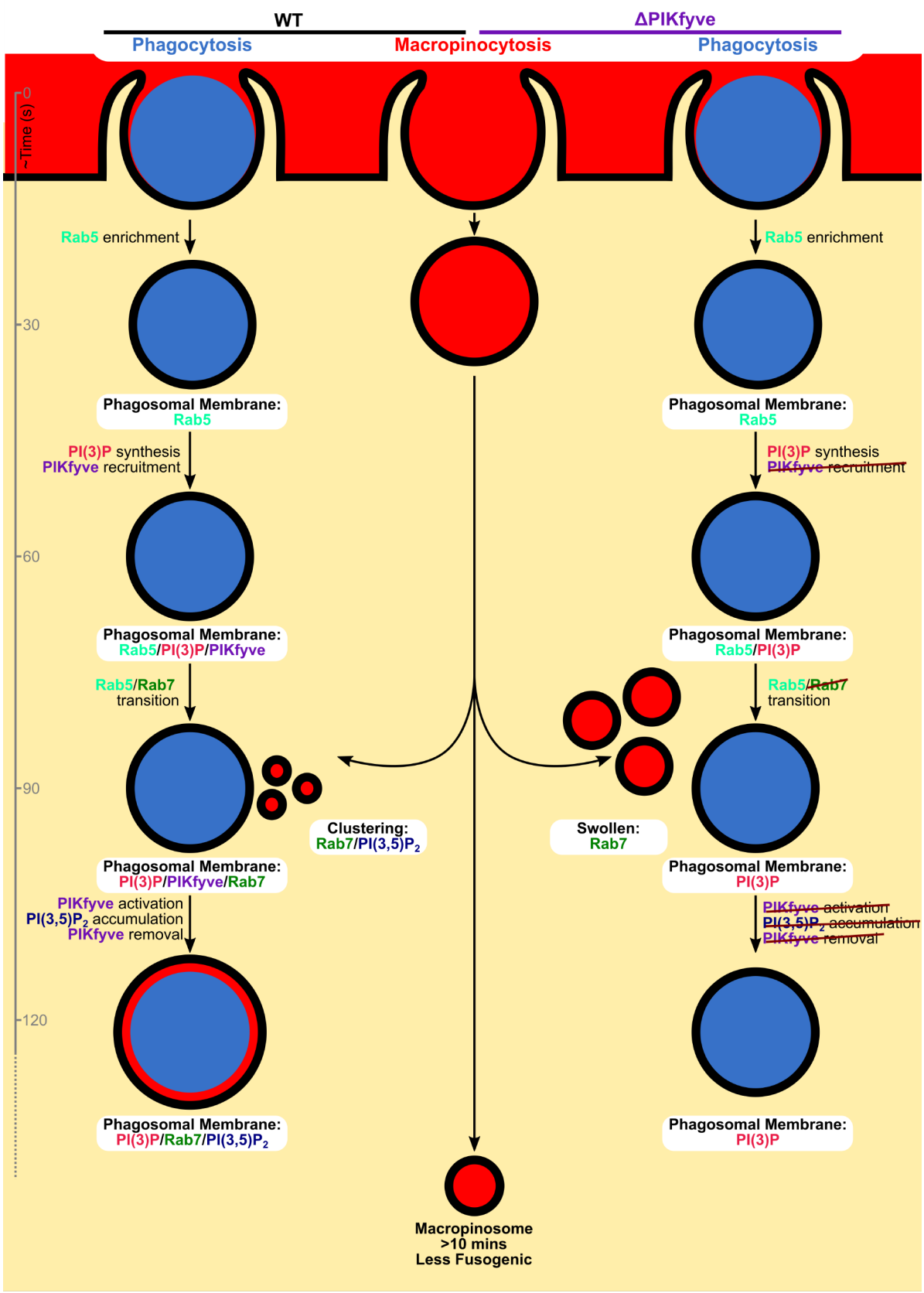

Figure 9: Model for the first 2 minutes of phagosome maturation. The left side indicates the maturation of phagosomes in wild-type cells, with PIKfyve-deficient cells on the right. Macropinosome maturation in the centre. Wild-type phagosomes accumulate each of the proteins and lipids indicated as per Figure 5G, with PIKfyve becoming activated ~ 1 minute after recruitment, at the point that macropinosomes of a similar age fuse and PIKfyve itself dissociates. In the absence of PIKfyve, macropinosomes do not shrink as efficiently, and do not cluster around, or fuse with phagosomes.

also be regulated. The crystal structure of the PIKfyve complex suggests that PIKfyve can be inhibited by auto-phosphorylation, requiring a protein dephosphorylation activity of Fig4 for activation (Lees et al., 2020). Fig4 may therefore be temporally regulated during phagosome maturation, or an additional unknown regulatory mechanism may exist. Our observations that PIKfyve normally dissociates as soon as PI(3,5)P2 accumulates but is retained if pharmacologically inactivated indicates that catalytic activity also affects membrane association. Catalytically inactive PIKfyve is also retained on macropinosomes in mammalian cells (Kerr et al., 2010). Whilst the FYVE domain is not well resolved in the crystal structure, it is suggested to lie near the kinase domain (Lees et al., 2020). This may provide potential for an additional level of regulation to explain the coordination of recruitment and activity *in vivo* but needs more investigation.

Our work demonstrates a key functional role for PIKfyve in phagosome maturation by mediating the delivery of multiple Rab7-positive compartments. Whilst some of these are PI(3,5)P2-containing macropinosomes, it is clear that other populations of vesicles also require PIKfyve for delivery. These include a population of small Rab7 vesicles that begin to cluster and fuse with nascent phagosomes almost immediately after internalisation. These appear to be completely absent in PIKfyve mutants, although Rab7-positive macropinosomes are retained (**Figure 2**). The source of these small, early-fusing vesicles is unclear but they may be classical lysosomes or late endosomes. We cannot distinguish between the loss of this compartment in its entirety or simply loss of its fusogenicity, but there is a general disruption in lysosomal fusion and regeneration in PIKfyve mutants, as shown by others (Choy et al., 2018; Jefferies et al., 2008; Nicot et al., 2006).

The observation that multiple populations of Rab7-positive vesicles fuse with phagosomes indicates a more complex picture than the canonical view of a single lysosomal population being delivered. Analyses of *Dictyostelium* phagosomes purified at different stages of maturation also showed different proteases were delivered and recovered over time (Gotthardt et al., 2006; Souza et al., 1997). The timescale in our experiments is much shorter but both studies implicate that multiple endosomal populations are involved in phagosome maturation. The sequential fusion of different endosomal and lysosomal populations was also observed in studies of macropinosome maturation in macrophages (Racoosin and Swanson, 1993) indicating that this is likely a universal phenomenon.

The observation that PI(3,5)P2-positive macropinosomes undergo continuous retrograde fusion with subsequent newly formed macropinosomes and phagosomes also challenges the view of maturation as a linear process. Our data indicate a more cyclic model whereby nascent macropinosomes fuse with a slightly older PI(3,5)P2-labelled population; then a proportion fuses again with the next round of macropinosomes whilst the rest progress further and lose fusogenicity and enter a terminally digestive phase (**Figure 9**). We speculate that these fusion events provide a mechanism to rapidly deliver a large volume of hydrolases, V-ATPase and other digestive machinery to newly internalised vesicles. Rapid enzyme delivery may be particularly important for both macropinosomes and phagosomes due to their large size and low surface area-to-volume ratio.

Studies in mammalian cells have also shown early macropinosomes fuse with one another in the first few minutes after formation, although it is unclear whether aged macropinosomes also possess this ability (Hamasaki et al., 2004; Schink et al., 2021). Fusion of macropinosomes with lysosomes is also at least partially regulated by recruitment of the septin cytoskeleton in a PIKfyve-dependent manner (Dolat and Spiliotis, 2016). *Dictyostelium* do not possess septins, which may explain why loss of PIKfyve does not appear to affect macropinosome digestion in these cells.

Fusion between macropinosomes and phagosomes has also been observed in mammalian cells and implicated during infection. Both *Salmonella enterica* and *Shigella flexineri* induce macropinosome formation from the ruffles they induce to drive entry into non-phagocytic host cells (Adam et al., 1996; Francis et al., 1993). These macropinosomes cluster around the bacteria-containing vacuole and appear to facilitate the rupture and escape of *Shigella* (Weiner et al., 2016) whereas they appear to stabilise and support the vacuolar lifestyle of *Salmonella* (Stevenin et al., 2019). Interestingly, inhibition of PIKfyve also disrupts *Salmonella* replication (Kerr et al., 2010). Whilst it is unclear how infection-associated macropinosomes relate to those made constitutively by professional phagocytes like macrophages or *Dictyostelium,* this highlights a common role for macropinosome delivery in the remodelling of microbe-containing compartments.

A further interesting aspect of our studies is the clear differences between phagosome and macropinosome maturation in *Dictyostelium*. Whilst early steps such as the Rab5-Rab7 transition and acquisition of PI(3)P followed by PI(3,5)P2 appear identical, macropinosomes

lose both phosphoinositides after 8 minutes, whilst phagosomes retain both throughout maturation and digestion. Furthermore, whilst PIKfyve is critical for phagosomal degradation, PIKfyve-deficient macropinosomes digest normally and still acquire Rab7, even though their shrinkage is reduced similar to observations in mammalian cells (Freeman et al., 2020; Kerr et al., 2010). The functions of PIKfyve in shrinkage and degradation therefore appear to be independent, and in *Dictyostelium* at least, only phagosomes require PIKfyve for Rab7 and lysosomal delivery. These differences are likely driven by signalling from phagocytic receptors, but how this is mediated and how it functionally affects killing and digestion remain unclear.

Many aspects of maturation are shared between phagosomes, macropinosomes, and other endocytic pathways, such as classical clathrin-mediated endosomes. These also transition from a Rab5/PI(3)P-positive early form to later compartments demarked by Rab7, V-ATPase and lysosomal components. Furthermore, degradation of classically endocytosed receptors, autophagosomes and entotic vesicles are also sensitive to PIKfyve inhibition (de Lartigue et al., 2009; Krishna et al., 2016; Qiao et al., 2021). While it is technically challenging to follow ~100nm endosomes in the detail possible with the much larger macropinosomes and phagosomes, it is likely that at least some of our observations are applicable to other endocytic routes. Here, we have harnessed an experimentally-tractable approach to define the complex and important sequence of events that occur in the first minutes of a phagosome. This approach has enabled key mechanistic insights in to the roles and regulation of PIKfyve and PI(3,5)P2, with important impact to generalized endocytic processes.

Acknowledgements

The authors thank Huaqing Cai for Rab expression plasmids, Douwe Veltman and Peggy Paschke for their continued development of his expression system and Robert Insall for his support in the early days of this project. DHM is supported by the Wellcome Trust grant 211193/Z/18/Z to and Royal Society RGS\R2\180284. AG and TS were supported by the Swiss National Science Foundation research grants 310030_149390, 310030_169386 and 310030_188813 to TS. JHV is funded by Royal Society grant RGF\EA\180126, JSK is funded by a Royal Society University Research Fellowship URF\R\201036. Imaging work was performed in the Wolfson Light Microscopy Facility at Sheffield.

Figure legends

Figure 1: PIKfyve is enriched on early macropinosome and phagosomes. (A) PIKfyve-GFP in wildtype *Dictyostelium* cells. PIKfyve is enriched on a peri-nuclear pool (pink arrow), and irregularly on the macropinosome membrane (pink star). (**B**) and (**C**) show PIKfyve-GFP localisation in ΔPIKfyve cells for increased contrast. Delivery to macropinosomes is shown in (**B**) with Alexa405-yeast containing phagosomes (blue) in (**C**). PIKfyve-GFP is delivered ~40 s post-formation and removed after 120 s. All scale bars = 2 µm.

Figure S3: Simultaneous analysis of RFP-Rab5 and GFP-Rab7 recruitment. Timelapse movies of **(A)** Wildtype and **(B)** ΔPIKfyve cells co-expressing RFP-Rab5A (magenta) and GFP-Rab7A (green) during phagocytosis of Alexa405-yeast (blue). Rab7A only arrives on wildtype phagosomes. The followed phagosome is indicted by and asterisk. All scale bars = 2 µm. The full timeseries is shown in Movie 7.

Figure 2: Loss of PIKfyve specifically affects Rab7 recruitment to phagosomes. Timelapse movies of **(A)** Wildtype and **(B)** ΔPIKfyve cells co-expressing RFP-Rab5A (magenta) and GFP-Rab7A (green) during phagocytosis of Alexa405-yeast (blue). The followed phagosome is indicted by and asterisk, see Movie 3 for full time series. RFP-Rab5A/GFP-Rab7A is clearly observed in wild-type cells, whilst ΔPIKfyve cells lose RFP-Rab5 normally, they fail to then accumulate GFP-Rab7A. Automated quantification of Rab5A and Rab7A recruitment to phagosomes is shown in **(C)** and **(D)** respectively, averaged over multiple movies when expressed individually as GFP-fusions. No significant differences in GFP-Rab5A enrichment were observed at any time points, but GFP-Rab7A was significantly decreased in ΔPIKfyve cells. (**E)** and **(F)** Representative timelapses of the PI(3)P reporter, GFP-2xFYVE, during phagocytosis of pHrodo-yeast (red) in wildtype and ΔPIKfyve cells. Pink arrows indicate GFP-2xFYVE labelled vesicles clustering around the phagosomal membrane from 30s. GFP-2xFYVE enrichment is quantified in (**G**). There were no statistically significant differences at any timepoints tested. (**H)** and **(I)** GFP-Rab7A recruitment to macropinosomes labelled by a 2 minute pulse of TxRed dextran (red) in wildtype and ΔPIKfyve cells. (**J)** Quantification by scoring the percentage of GFP-positive macropinosomes at each time point after dextran wash out. GFP-Rab7A dynamics are similar

in both cell types. Data shown throughout are the mean ± SEM of 3 independent experiments, with N indicating the total number of cells measured. The means of each independent repeat are indicated by the additional thin lines in C,D and J and the crosses in J. Statistical significances in C, D and J were calculated by unpaired T-test of a 5-point rolling average. The purple arrow on each graph indicates the time of GFP-PIKfyve arrival. All scale bars = 2 µm.

Figure 3: Identification of SnxA as a PI(3,5)P_2 reporter. (A) and **(B)** Expression of GFP-fusions of PX-domain containing proteins in wildtype and ΔPIKfyve Ax3 *Dictyostelium*. (**A**) DDB_G0285711 localised to large vesicles in both cells, whereas DDB_G0289833 (**B**) was completely cytosolic in ΔPIKfyve. (**C**) Timelapse of DDB_G0289833 (SnxA)-GFP localistion in Ax2 cells after addition of the PIKfyve inhibitor apilimod (3µM). Quantification of number of SnxA-GFP vesicles per cell is shown in (**D**). >90 cells measured per time-point. Data shows mean ± SEM of 3 independent experiments. (**E**) PIP array using lysates from wildtype cells expressing SnxA-GFP and probed with anti-GFP antibody. (**F**) Schematics of SnxA-GFP, 1xPX-GFP and 2xPX-GFP. (**G**) Representative images of their localisation in the cells indicated. 1xPX-GFP remained predominately cytosolic in wildtype cells, whereas 2xPX-GFP localised strongly to large vesicles, which was lost in ΔPIKfyve and apilimod treated cells. All scale bars = 2 µm.

Figure 4: PI(3,5)P_2 binding specificity. (A-D) Representative images and quantification of recombinant GFP-SnxA probes to membrane coated beads containing the indicated PIPs. (**E**) Binding of each SnxA probe titrated against beads harboring PI(3,5)P2. Intensities and apparent K_ds are shown in (**F**). All graphs show the mean ± standard deviation from 3 independent experiments.

Figure 5: PI(3,5)P_2 dynamics during macropinosome and phagosome maturation. (A) and **(B)** Timelapses of SnxA-GFP during phagocytosis of pHrodo-yeast (red) in wildtype (**A**) and ΔPIKfyve (**B**) cells. Pink arrowheads indicates clustering SnxA vesicles. (**C**) Quantification of SnxA-GFP enrichment at the phagosomal membrane for 51 wildtype and 31 ΔPIKfyve phagosomes across 3 independent experiments. Fold enrichment normalised to 10s before engulfment. Purple arrow indicates time of PIKfyve arrival from Figure 1. (**D**) Timelapse of SnxA-GFP recruitment to a newly formed macropinosome (marked by asterisk). Pink arrowheads indicate clustered vesicles prior to fusion. (**E**) Longer-term

imaging of SnxA-GFP recruitment to macropinosomes via a 2 minute dextran pulse-chase. Different fields of view were taken at time points after dextran wash-out. The proportion of SnxA-GFP positive macropinosomes at each time after dextran addition is shown in (**F**). >40 vesicles were counted per time-point across 3 independent experiments. Both graphs show the mean ± SEM of 3 independent experiments. All scale bars = 2 μm. (**G**) Schematic summary of the dynamics of each component studied on the phagosomal membrane.

Figure 6: Regulation of PIKfyve activity and recruitment. (A) Timelapse of cells coexpressing 2xPX-RFP (magenta) and PIKfyve-GFP (green) during phagocytosis of Alexa405-yeast (blue). (**B**) Fluorescence intensity around the phagosome in (**A**). Data shown is the mean intensity ± the standard deviation around the phagosomal membrane normalised between minimum and maximum intensities observed. **(C)** and **(D)** Timelapse of PIKfyve-GFP during phagocytosis of pHrodo-yeast (red) in cells before (**C**) and after (**D**) addition of 5μM apilimod. The PIKfyve-GFP intensity around the phagosome in these movies is quantified in (**E**). (**F**) Shows the PIKfyve-GFP dynamics over multiple events, by manually scoring the time of PIKfyve-GFP delivery and release. 14 untreated events and 10 apilimod treated events were scored and the thick line indicates the proportion of GFP-positive phagosomes at each time after engulfment. Thin lines represent individual events. All scale bars = 2 μm.

Figure 7: SnxA is delivered after Rab7 and VatM. (A) Timelapses of RFP-Rab7A (magenta) and SnxA-GFP (green) during phagocytosis of Alexa405-yeast (blue) in wildtype cells. SnxA and Rab7 co-localize on many clustering vesicles (arrowheads) (**B**) Timelapse of VatM-RFP (magenta) and SnxA-GFP (green) during phagocytosis of Alexa405-yeast (blue). Fluorescence intensity around phagosomes in A and B, are shown in (**C**) and **(D)** respectively. Data is mean intensity ± SD of a linescan along the phagosomal membrane normalised between minimum and maximum intensities observed**.**

Figure 8: PIKfyve drives fusion between macropinosomes and phagosomes. (A) and (**B**) Timelapses of interactions between early (<5mins) macropinosomes (red) and phagosomes (blue) in wildtype and ΔPIKfyve cells, after sequential addition of fluorescent dextran and yeast. Schematic shows experimental procedure. Macropinosomes cluster around phagosomes in wildtype but not in ΔPIKfyve cells. (**C**) Quantification of dextran intensity around phagosomes, averaged over multiple events. Graph shows fold enrichment

normalised to 10s before engulfment ± SEM. (**D)** TxRed-dextran (red) accumulation within the phagosomal membrane (green) marked by 2xFYVE (arrowhead). (**E**) Shows the same, using a budded yeast. Note strong dextran accumulation around the bud neck (dashed box). (**F)** Quantification of dextran intensity in this area averaged across multiple events ± SEM, binned by the age of the phagosome. **(G-I)** Images and quantification of clustering macropinosome identity. Wildtype cells expressing GFP-Rab7A, GFP-2xFYVE or SnxA-GFP were treated with a dextran pulse-chase before phagocytosis of yeast. Macropinosomes within 1 μm of the phagosome were identified at each timepoint and both total number (red bars) and proportion colocalizing with the respective GFP-reporter (green bars and numbers) were scored manually. Frames were binned into 2- minute groups, data shown are the mean ±SEM of three independent experiments. Note increased clustering from 2 minutes, with high Rab7 colocalization, followed by an increase in SnxA-GFP positive macropinosomes after 4 mins. (**J)** Quantification of dextran delivery (as in F) after a 10-minute delay before addition of yeast (see schematic, same control data as in F). Older macropinosomes show less delivery to phagosomes. All purple arrows on graphs indicate the time of PIKfyve arrival. All scale bars = 2 μm.

Figure 9: Model for the first 2 minutes of phagosome maturation. The left side indicates the maturation of phagosomes in wild-type cells, with PIKfyve-deficient cells on the right. Macropinosome maturation in the centre. Wild-type phagosomes accumulate each of the proteins and lipids indicated as per Figure 5G, with PIKfyve becoming activated ~ 1 minute after recruitment, at the point that macropinosomes of a similar age fuse and PIKfyve itself dissociates. In the absence of PIKfyve, macropinosomes do not shrink as efficiently, and do not cluster around, or fuse with phagosomes.

Figure S1: PIKfyve-GFP expression rescues the swollen endosomes in ΔPIKfyve cells. **A:** Wildtype, ΔPIKfyve, and PIKfyve rescued cells grown in TxRed dextran. Swollen endosomes (likely macropinosomes) are only present in ΔPIKfyve cells. All scale bars = 2 µm. (**B**) Shows automated methodology to quantify fluorescent reporter recruitment to a phagocytic event. Channel containing yeast (red) is thresholded and particles larger than 1.5 μm^2 are segmented (white circles). This area is used to monitor fluorescence change of pHrodo-labelled-yeast, a proxy for phagosomal pH, shown in (**C**). The perimeter is enlarged by 0.2 µm to generate a ring of 0.3 µm thickness over the phagosomal membrane (inner ring). As a control, and additional ring further away from the yeast (outer ring, expanded by 0.85 µm from the yeast) was also generated, to give a measure of background cytosol fluorescence that should remain constant. (**D**) Shows the quantification of the representative movie in panel B.

Figure S2: Delivery of reporters to phagosomes and macropinosomes. (A) and **(B)** Representative timelapses of GFP-Rab5A during phagocytosis of pHrodo-yeast (red) in wildtype (**A**) and ΔPIKfyve (**B**) cells. **(C)** and **(D)** show equivalent movies of GFP-Rab7A, see **Movies 5 and 6** for full time series. **(E)** Expression levels of GFP-reporter levels in wildtype and ΔPIKfyve cells. Western blot of whole cell lysates probed with anti-GFP antibody. Streptavidin staining of endogenously biotinylated proteins used as loading control. (**F**) and (**G**) Long-term timelapses of GFP-2xFYVE and GFP-Rab7A recruitment to phagosomes. Both reporters remain associated for at least 1 hour after engulfment. The time each event could be tracked varied due to the point in the timelapse at which engulfment occurred but the proportion of phagosomes still positive for each reporter at the end of each movie is shown in (**H**). Only those able to be tracked for >30 minutes were scored. **(I)** Quantification of macropinosome shrinkage during early maturation. Images of the cell lines indicated were taken at timepoints after a 2-minute TRITC dextran-pulse chase and macropinosomes size quantified automatically. Whilst wild-type macropinosomes lose ~ half their volume within 5 minutes, this is disrupted in ΔPIKfyve cells. Graph represents the mean ± SEM of six independent experiments. Biological replicates shown by crosses. (**J**) Fluid phase proteolytic activity in wildtype and ΔPIKfyve cells measured by increase in fluorescence after a 2-minute pulse of DQ-BSA. Data shown is mean ± SD of three independent experiments.

Figure S3: SnxA does not bind PI(5)P. (A) PIP array performed using lysates from wildtype cells expressing 2xPX-GFP and probed with anti-GFP antibody. (**B)** Coomassie stained SDS-PAGE gels of recombinant GFP fusion SnxA probes used for lipid binding assays. **(C)** Representative images of SnxA probe titrated against PI(5)P-containing membrane coated beads. Quantified in **(D)**.

Figure S4: Loss of SnxA has little effect on phagosome or macropinosome maturation. (**A)** Images of wildtype and ΔsnxA-1 colonies growing on a lawn of *K. aerogenes*. Average colony diameter over time is shown below. Scale bar = 10mm. **(B)** Growth of mutant cells in different bacteria. Numbers indicate the number of *Dictyostelium* cells seeded on each well. (**C)** Summary of growth on a range of bacteria screened as in (**B**). (**D)** Quantification of endocytosis calculated by FITC dextran uptake. (**E)** Phagocytosis of 1 µm fluorescent beads, measured by flow cytometry and normalised to wildtype cells at 60 mins. (**F)** Phagosomal proteolysis and **(G)** pH over time, measured by fluorescence changes after engulfment of either DQ-BSA or FITC/Alexa594 reporter beads respectively. (**H)** Representative images of macropinosomes shrinking after a 2 minute pulse of TRITC-dextran, Scale bar = 2 µm. Size is quantified in (**I).** All data shown are the mean± SD of at least 3 independent experiments. ΔsnxA-1, 2 and 3 indicate independent knockout clones.

Figure S5: SnxA-GFP localization. (A) Extended timelapse of SnxA-GFP localisation to phagosomes containing Alexa405-yeast (blue). (**B)** Quantification of SnxA-GFP localisation to phagosomes. SnxA-GFP was manually scored as on or off over 60 minutes for 20 phagocytosis events. Thin lines represent individual events, and thick line represents mean percentage localisation. (**C)** and **(D)** Timelapses of cells coexpressing 2xFYVE-RFP (magenta) and SnxA-GFP (green) during macropinocytosis and phagocytosis respectively. The macropinosome/phagosome followed is indicated with an asterisk. See Movie 9 for full time series. All scale bars = 2 µm.

Figure S6: Macropinosome maturation and fusion. (A) Timelapse of RFP-Rab7A (magenta) and SnxA-GFP (green) during macropinosome maturation. Rab7 arrives before SnxA and co-localize on some clustering vesicles. (**B)** Timelapse of cells after sequential pulses of TxRed and FITC dextran. The older macropinosomes (red) can be seen fusing and mixing contents with a newly formed macropinosome (yellow). All scale bars = 2 µm.

Movie legends

Movie 1: Recruitment of GFP-PIKfyve, to a newly formed macropinosome (asterisk). GFP-PIKfyve expressed in a ΔPIKfyve cell. Scale bar = 2 µm

Movie 2: Recruitment of GFP-PIKfyve, to phagosomes. Engulfment of an alexa405-labelled yeast by a GFP-PIKfyve expressing ΔPIKfyve cell. Scale bar = 2 µm

Movie 3: Simultaneous imaging of RFP-Rab5A and GFP-Rab7A recruitment to phagosomes in wild-type (top) and ΔPIKfyve (bottom) cells. Scale bar = 2 µm

Movie 4: Enrichment of GFP-Rab5A at phagocytic cups. Multiple failed attempts to complete engulfment of a pHrodo labelled yeast demonstrate that GFP-Rab5A is enriched at the cup before internalisation completes. Scale bar = 2 µm

Movie 5: GFP-Rab5A dynamics at phagosomes in both wildtype (left) and ΔPIKfyve (right) cells. Scale bar = 2 µm

Movie 6: GFP-Rab7A dynamics at phagosomes in both wildtype (left) and ΔPIKfyve (right) cells. Scale bar = 2 µm

Movie 7: PI(3)P dynamics at phagosomes in both wildtype (left) and ΔPIKfyve (right) cell. Cells expressing GFP-2xFYVE reporter for PI(3)P. Scale bar = 2 µm

Movie 8: PI(3,5)P2 dynamics during phagosome maturation. Wildtype (left) and ΔPIKfyve (right) cells expressing the SnxA-GFP probe for PI(3,5)P2 . Note the complete loss of localisation in the mutants. Scale bar = 2 µm

Movie 9: Simultaneous imaging of PI(3)P (RFP-2xFYVE, magenta) and PI(3,5)P2 (SnxA-GFP) recruitment to phagosomes in wildtype cells. Scale bar = 2 µm

Movie 10: Simultaneous imaging of PIKfyve-GFP and PI(3,5)P2 formation (RFP-2xPX, in magenta), in wildtype cells. Scale bar = 2 µm

References

Adam, T., Giry, M., Boquet, P. and Sansonetti, P. (1996). Rho-dependent membrane folding causes Shigella entry into epithelial cells. *EMBO J* **15**, 3315-21.

Benghezal, M., Fauvarque, M., Tournebize, R., Froquet, R., Marchetti, A., Bergeret, E., Lardy, B., Klein, G., Sansonetti, P., Charette, S. et al. (2006). Specific host genes required for the killing of Klebsiella bacteria by phagocytes. *Cell Microbiol* **8**, 139-48.

Berwick, D. C., Dell, G. C., Welsh, G. I., Heesom, K. J., Hers, I., Fletcher, L. M., Cooke, F. T. and Tavare, J. M. (2004). Protein kinase B phosphorylation of PIKfyve regulates the trafficking of GLUT4 vesicles. *J Cell Sci* **117**, 5985-93.

Bonangelino, C. J., Nau, J. J., Duex, J. E., Brinkman, M., Wurmser, A. E., Gary, J. D., Emr, S. D. and Weisman, L. S. (2002). Osmotic stress-induced increase of phosphatidylinositol 3,5-bisphosphate requires Vac14p, an activator of the lipid kinase Fab1p. *J Cell Biol* **156**, 1015-28.

Botelho, R. J., Efe, J. A., Teis, D. and Emr, S. D. (2008). Assembly of a Fab1 Phosphoinositide Kinase Signaling Complex Requires the Fig4 Phosphoinositide Phosphatase. *Molecular Biology of the Cell* **19**, 4273-4286.

Buckley, C. M., Gopaldass, N., Bosmani, C., Johnston, S. A., Soldati, T., Insall, R. H. and King, J. S. (2016). WASH drives early recycling from macropinosomes and phagosomes to maintain surface phagocytic receptors. *Proc Natl Acad Sci U S A* **113**, E5906-E5915.

Buckley, C. M., Heath, V. L., Gueho, A., Bosmani, C., Knobloch, P., Sikakana, P., Personnic, N., Dove, S. K., Michell, R. H., Meier, R. et al. (2019). PIKfyve/Fab1 is required for efficient V-ATPase and hydrolase delivery to phagosomes, phagosomal killing, and restriction of Legionella infection. *PLoS Pathog* **15**, e1007551.

Buczynski, G., Bush, J., Zhang, L., Rodriguez-Paris, J. and Cardelli, J. (1997). Evidence for a recycling role for Rab7 in regulating a late step in endocytosis and in retention of lysosomal enzymes in Dictyostelium discoideum. *Mol Biol Cell* **8**, 1343-60.

Cabezas, A., Pattni, K. and Stenmark, H. (2006). Cloning and subcellular localization of a human phosphatidylinositol 3-phosphate 5-kinase, PIKfyve/Fab1. *Gene* **371**, 34-41.

Cai, X., Xu, Y., Cheung, A. K., Tomlinson, R. C., Alcazar-Roman, A., Murphy, L., Billich, A., Zhang, B., Feng, Y., Klumpp, M. et al. (2013). PIKfyve, a class III PI kinase, is the target of the small molecular IL-12/IL-23 inhibitor apilimod and a player in Toll-like receptor signaling. *Chem Biol* **20**, 912-21.

Calvo-Garrido, J., King, J. S., Munoz-Braceras, S. and Escalante, R. (2014). Vmp1 regulates PtdIns3P signaling during autophagosome formation in Dictyostelium discoideum. *Traffic* **15**, 1235-46.

Chen, D., Xiao, H., Zhang, K., Wang, B., Gao, Z., Jian, Y., Qi, X., Sun, J., Miao, L. and Yang, C. (2010). Retromer is required for apoptotic cell clearance by phagocytic receptor recycling. *Science* **327**, 1261-4.

Chen, Z., Malia, P. C., Hatakeyama, R., Nicastro, R., Hu, Z., Peli-Gulli, M. P., Gao, J., Nishimura, T., Eskes, E., Stefan, C. J. et al. (2021). TORC1 Determines Fab1 Lipid Kinase Function at Signaling Endosomes and Vacuoles. *Curr Biol* **31**, 297-309 e8.

Choy, C. H., Saffi, G., Gray, M. A., Wallace, C., Dayam, R. M., Ou, Z. A., Lenk, G., Puertollano, R., Watkins, S. C. and Botelho, R. J. (2018). Lysosome enlargement during inhibition of the lipid kinase PIKfyve proceeds through lysosome coalescence. *J Cell Sci* **131**.

Christoforidis, S., Miaczynska, M., Ashman, K., Wilm, M., Zhao, L. Y., Yip, S. C., Waterfield, M. D., Backer, J. M. and Zerial, M. (1999). Phosphatidylinositol-3-OH kinases are Rab5 effectors. *Nature Cell Biology* **1**, 249-252.

Cosson, P., Zulianello, L., Join-Lambert, O., Faurisson, F., Gebbie, L., Benghezal, M., Van Delden, C., Curty, L. and Kohler, T. (2002). Pseudomonas aeruginosa virulence analyzed in a Dictyostelium discoideum host system. *J Bacteriol* **184**, 3027-33.

Davidson, A. J., King, J. S. and Insall, R. H. (2013). The use of streptavidin conjugates as immunoblot loading controls and mitochondrial markers for use with Dictyostelium discoideum. *BioTechniques* **55**, 39-41.

Dayam, R. M., Saric, A., Shilliday, R. E. and Botelho, R. J. (2015). The Phosphoinositide-Gated Lysosomal Ca(2+) Channel, TRPML1, Is Required for Phagosome Maturation. *Traffic* **16**, 1010-26.

Dayam, R. M., Sun, C. X., Choy, C. H., Mancuso, G., Glogauer, M. and Botelho, R. J. (2017). The Lipid Kinase PIKfyve Coordinates the Neutrophil Immune Response through the Activation of the Rac GTPase. *J Immunol* **199**, 2096-2105.

de Lartigue, J., Polson, H., Feldman, M., Shokat, K., Tooze, S. A., UrbÃ©, S. and Clague, M. J. (2009). PIKfyve Regulation of Endosome-Linked Pathways. *Traffic* **10**, 883-893.

Demirsoy, S., Martin, S., Motamedi, S., van Veen, S., Holemans, T., Van den Haute, C., Jordanova, A., Baekelandt, V., Vangheluwe, P. and Agostinis, P. (2017). ATP13A2/PARK9 regulates endo-/lysosomal cargo sorting and proteostasis through a novel PI(3, 5)P2-mediated scaffolding function. *Hum Mol Genet*.

Dolat, L. and Spiliotis, E. T. (2016). Septins promote macropinosome maturation and traffic to the lysosome by facilitating membrane fusion. *J Cell Biol* **214**, 517-27.

Dong, X. P., Shen, D., Wang, X., Dawson, T., Li, X., Zhang, Q., Cheng, X., Zhang, Y., Weisman, L. S., Delling, M. et al. (2010). PI(3,5)P(2) controls membrane trafficking by direct activation of mucolipin Ca(2+) release channels in the endolysosome. *Nat Commun* **1**, 38.

Dove, S. K., Dong, K., Kobayashi, T., Williams, F. K. and Michell, R. H. (2009). Phosphatidylinositol 3,5-bisphosphate and Fab1p/PIKfyve underPPIn endo-lysosome function. *Biochem J* **419**, 1-13.

Ferguson, C. J., Lenk, G. M. and Meisler, M. H. (2009). Defective autophagy in neurons and astrocytes from mice deficient in PI(3,5)P2. *Hum Mol Genet* **18**, 4868-78.

Fey, P., Dodson, R. J., Basu, S. and Chisholm, R. L. (2013). One stop shop for everything Dictyostelium: dictyBase and the Dicty Stock Center in 2012. *Methods Mol Biol* **983**, 59-92.

Francis, C. L., Ryan, T. A., Jones, B. D., Smith, S. J. and Falkow, S. (1993). Ruffles induced by Salmonella and other stimuli direct macropinocytosis of bacteria. *Nature* **364**, 639-42.

Freeman, S. A., Uderhardt, S., Saric, A., Collins, R. F., Buckley, C. M., Mylvaganam, S., Boroumand, P., Plumb, J., Germain, R. N., Ren, D. et al. (2020). Lipid-gated monovalent ion fluxes regulate endocytic traffic and support immune surveillance. *Science* **367**, 301-305.

Froquet, R., Lelong, E., Marchetti, A. and Cosson, P. (2009). Dictyostelium discoideum: a model host to measure bacterial virulence. *Nat Protoc* **4**, 25-30.

Gerisch, G. (1959). Ein submerskulturver fahren fur entwicklungsphysiologische untersuchungen an Dictyostelium discoideum. *Naturwissenschaften* **46**, 654–656.

Gillooly, D., Morrow, I., Lindsay, M., Gould, R., Bryant, N., Gaullier, J., Parton, R. and Stenmark, H. (2000). Localization of phosphatidylinositol 3-phosphate in yeast and mammalian cells. *EMBO J* **19**, 4577-88.

Gotthardt, D., Blancheteau, V., Bosserhoff, A., Ruppert, T., Delorenzi, M. and Soldati, T. (2006). Proteomics fingerprinting of phagosome maturation and evidence for the role of a Galpha during uptake. *Mol Cell Proteomics* **5**, 2228-43.

Gutierrez, M. G. (2013). Functional role(s) of phagosomal Rab GTPases. *Small GTPases* **4**, 148-58.

Hamasaki, M., Araki, N. and Hatae, T. (2004). Association of early endosomal autoantigen 1 with macropinocytosis in EGF-stimulated A431 cells. *Anat Rec A Discov Mol Cell Evol Biol* **277**, 298-306.

Hammond, G. R., Takasuga, S., Sasaki, T. and Balla, T. (2015). The ML1Nx2 Phosphatidylinositol 3,5-Bisphosphate Probe Shows Poor Selectivity in Cells. *PLoS One* **10**, e0139957.

Ikonomov, O., Sbrissa, D. and Shisheva, A. (2001). Mammalian cell morphology and endocytic membrane homeostasis require enzymatically active phosphoinositide 5-kinase PIKfyve. *J Biol Chem* **276**, 26141-7.

Ikonomov, O. C., Sbrissa, D., Fenner, H. and Shisheva, A. (2009). PIKfyve-ArPIKfyve-Sac3 core complex: contact sites and their consequence for Sac3 phosphatase activity and endocytic membrane homeostasis. *J Biol Chem* **284**, 35794-806.

Isobe, Y., Nigorikawa, K., Tsurumi, G., Takemasu, S., Takasuga, S., Kofuji, S. and Hazeki, K. (2019). PIKfyve accelerates phagosome acidification through activation of TRPML1 while arrests aberrant vacuolation independent of the Ca2+ channel. *J Biochem* **165**, 75-84.

Jefferies, H. B., Cooke, F. T., Jat, P., Boucheron, C., Koizumi, T., Hayakawa, M., Kaizawa, H., Ohishi, T., Workman, P., Waterfield, M. D. et al. (2008). A selective PIKfyve inhibitor blocks PtdIns(3,5)P(2) production and disrupts endomembrane transport and retroviral budding. *EMBO Rep* **9**, 164-70.

Kerr, M. C., Lindsay, M. R., Luetterforst, R., Hamilton, N., Simpson, F., Parton, R. G., Gleeson, P. A. and Teasdale, R. D. (2006). Visualisation of macropinosome maturation by the recruitment of sorting nexins. *J Cell Sci* **119**, 3967-80.

Kerr, M. C., Wang, J. T., Castro, N. A., Hamilton, N. A., Town, L., Brown, D. L., Meunier, F. A., Brown, N. F., Stow, J. L. and Teasdale, R. D. (2010). Inhibition of the PtdIns (5) kinase PIKfyve disrupts intracellular replication of Salmonella. *The EMBO journal* **29**, 1331-1347.

Kim, G. H., Dayam, R. M., Prashar, A., Terebiznik, M. and Botelho, R. J. (2014). PIKfyve Inhibition Interferes with Phagosome and Endosome Maturation in Macrophages. *Traffic* **15**, 1143-63.

King, J. S. and Kay, R. R. (2019). The origins and evolution of macropinocytosis. *Philos Trans R Soc Lond B Biol Sci* **374**, 20180158.

Krishna, S., Palm, W., Lee, Y., Yang, W., Bandyopadhyay, U., Xu, H., Florey, O., Thompson, C. B. and Overholtzer, M. (2016). PIKfyve Regulates Vacuole Maturation and Nutrient Recovery following Engulfment. *Dev Cell* **38**, 536-47.

Lees, J. A., Li, P., Kumar, N., Weisman, L. S. and Reinisch, K. M. (2020). Insights into Lysosomal PI(3,5)P2 Homeostasis from a Structural-Biochemical Analysis of the PIKfyve Lipid Kinase Complex. *Mol Cell* **80**, 736-743 e4.

Leray, X., Hilton, J. K., Nwangwu, K., Becerril, A., Mikusevic, V., Fitzgerald, G., Amin, A., Weston, M. R. and Mindell, J. A. (2022). Tonic inhibition of the chloride/proton antiporter ClC-7 by PI(3,5)P2 is crucial for lysosomal pH maintenance. *Elife* **11**.

Levin, R., Grinstein, S. and Canton, J. (2016). The life cycle of phagosomes: formation, maturation, and resolution. *Immunol Rev* **273**, 156-79.

Li, S. C., Diakov, T. T., Xu, T., Tarsio, M., Zhu, W., Couoh-Cardel, S., Weisman, L. S. and Kane, P. M. (2014). The signaling lipid PI(3,5)P(2) stabilizes V(1)-V(o) sector interactions and activates the V-ATPase. *Mol Biol Cell* **25**, 1251-62.

Li, X., Rydzewski, N., Hider, A., Zhang, X., Yang, J., Wang, W., Gao, Q., Cheng, X. and Xu, H. (2016). A molecular mechanism to regulate lysosome motility for lysosome positioning and tubulation. *Nat Cell Biol* **18**, 404-17.

Li, X., Wang, X., Zhang, X., Zhao, M., Tsang, W. L., Zhang, Y., Yau, R. G., Weisman, L. S. and Xu, H. (2013). Genetically encoded fluorescent probe to visualize intracellular phosphatidylinositol 3,5-bisphosphate localization and dynamics. *Proc Natl Acad Sci U S A* **110**, 21165-70.

Maib, H. and Murray, D. H. (2022). A mechanism for exocyst-mediated tethering via Arf6 and PIP5K1C-driven phosphoinositide conversion. *Curr Biol*.

Maniak, M. (2001). Fluid-phase uptake and transit in axenic Dictyostelium cells. *Biochim Biophys Acta* **1525**, 197-204.

McCartney, A. J., Zhang, Y. and Weisman, L. S. (2014a). Phosphatidylinositol 3,5-bisphosphate: low abundance, high significance. *Bioessays* **36**, 52-64.

McCartney, A. J., Zolov, S. N., Kauffman, E. J., Zhang, Y., Strunk, B. S., Weisman, L. S. and Sutton, M. A. (2014b). Activity-dependent PI(3,5)P2 synthesis controls AMPA receptor trafficking during synaptic depression. *Proc Natl Acad Sci U S A* **111**, E4896-905.

Neuhaus, E., Almers, W. and Soldati, T. (2002). Morphology and dynamics of the endocytic pathway in Dictyostelium discoideum. *Mol Biol Cell* **13**, 1390-407.

Nicot, A. S., Fares, H., Payrastre, B., Chisholm, A. D., Labouesse, M. and Laporte, J. (2006). The phosphoinositide kinase PIKfyve/Fab1p regulates terminal lysosome maturation in Caenorhabditis elegans. *Mol Biol Cell* **17**, 3062-74.

Paschke, P., Knecht, D. A., Silale, A., Traynor, D., Williams, T. D., Thomason, P. A., Insall, R. H., Chubb, J. R., Kay, R. R. and Veltman, D. M. (2018). Rapid and efficient genetic engineering of both wild type and axenic strains of Dictyostelium discoideum. *PLoS One* **13**, e0196809.

Poteryaev, D., Datta, S., Ackema, K., Zerial, M. and Spang, A. (2010). Identification of the switch in early-to-late endosome transition. *Cell* **141**, 497-508.

Qiao, Y., Choi, J. E., Tien, J. C., Simko, S. A., Rajendiran, T., Vo, J. N., Delekta, A. D., Wang, L., Xiao, L., Hodge, N. B. et al. (2021). Autophagy Inhibition by Targeting PIKfyve Potentiates Response to Immune Checkpoint Blockade in Prostate Cancer. *Nat Cancer* **2**, 978-993.

Racoosin, E. L. and Swanson, J. A. (1993). Macropinosome maturation and fusion with tubular lysosomes in macrophages. *J Cell Biol* **121**, 1011-20.

Ratner, D. and Newell, P. (1978). Linkage analysis in Dictyostelium discoideum using multiply marked tester strains: establishment of linkage group VII and the reassessment of earlier linkage data. *J Gen Microbiol* **109**, 225-36.

Rink, J., Ghigo, E., Kalaidzidis, Y. and Zerial, M. (2005). Rab conversion as a mechanism of progression from early to late endosomes. *Cell* **122**, 735-749.

Rudge, S. A., Anderson, D. M. and Emr, S. D. (2004). Vacuole size control: regulation of PtdIns(3,5)P2 levels by the vacuole-associated Vac14-Fig4 complex, a PtdIns(3,5)P2-specific phosphatase. *Mol Biol Cell* **15**, 24-36.

Rusten, T. E., Rodahl, L. M., Pattni, K., Englund, C., Samakovlis, C., Dove, S., Brech, A. and Stenmark, H. (2006). Fab1 phosphatidylinositol 3-phosphate 5-kinase controls trafficking but not silencing of endocytosed receptors. *Mol Biol Cell* **17**, 3989-4001.

Samie, M., Wang, X., Zhang, X. L., Goschka, A., Li, X. R., Cheng, X. P., Gregg, E., Azar, M., Zhuo, Y., Garrity, A. G. et al. (2013). A TRP Channel in the Lysosome Regulates Large Particle Phagocytosis via Focal Exocytosis. *Developmental Cell* **26**, 511-524.

Sattler, N., Monroy, R. and Soldati, T. (2013). Quantitative analysis of phagocytosis and phagosome maturation. *Methods Mol Biol* **983**, 383-402.

Sbrissa, D., Ikonomov, O. C., Fu, Z. Y., Ijuin, T., Gruenberg, J., Takenawa, T. and Shisheva, A. (2007). Core protein machinery for mammalian phosphatidylinositol 3,5-bisphosphate synthesis and turnover that regulates the progression of endosomal transport - Novel sac phosphatase joins the arpikfyve-pikfyve complex. *Journal of Biological Chemistry* **282**, 23878-23891.

Sbrissa, D., Ikonomov, O. C. and Shisheva, A. (1999). PIKfyve, a mammalian ortholog of yeast Fab1p lipid kinase, synthesizes 5-phosphoinositides. Effect of insulin. *J Biol Chem* **274**, 21589-97.

Sbrissa, D., Ikonomov, O. C. and Shisheva, A. (2000). PIKfyve lipid kinase is a protein kinase: downregulation of 5'-phosphoinositide product formation by autophosphorylation. *Biochemistry* **39**, 15980-9.

Schink, K. O., Tan, K. W., Spangenberg, H., Martorana, D., Sneeggen, M., Stevenin, V., Enninga, J., Campsteijn, C., Raiborg, C. and Stenmark, H. (2021). The phosphoinositide coincidence detector Phafin2 promotes macropinocytosis by coordinating actin organisation at forming macropinosomes. *Nat Commun* **12**, 6577.

Shisheva, A. (2012). PIKfyve and its Lipid products in health and in sickness. *Curr Top Microbiol Immunol* **362**, 127-62.

Smith, A. C., Heo, W. D., Braun, V., Jiang, X., Macrae, C., Casanova, J. E., Scidmore, M. A., Grinstein, S., Meyer, T. and Brumell, J. H. (2007). A network of Rab GTPases controls phagosome maturation and is modulated by Salmonella enterica serovar Typhimurium. *J Cell Biol* **176**, 263-8.

Souza, G. M., Mehta, D. P., Lammertz, M., Rodriguez-Paris, J., Wu, R., Cardelli, J. A. and Freeze, H. H. (1997). Dictyostelium lysosomal proteins with different sugar modifications sort to functionally distinct compartments. *J Cell Sci* **110 (Pt 18)**, 2239-48.

Stevenin, V., Chang, Y. Y., Le Toquin, Y., Duchateau, M., Gianetto, Q. G., Luk, C. H., Salles, A., Sohst, V., Matondo, M., Reiling, N. et al. (2019). Dynamic Growth and Shrinkage of the Salmonella-Containing Vacuole Determines the Intracellular Pathogen Niche. *Cell Rep* **29**, 3958-3973 e7.

Tu, H., Wang, Z., Yuan, Y., Miao, X., Li, D., Guo, H., Yang, Y. and Cai, H. (2022). The PripA-TbcrA complex-centered Rab GAP cascade facilitates macropinosome maturation in Dictyostelium. *Nat Commun* **13**, 1787.

Veltman, D. M., Akar, G., Bosgraaf, L. and Van Haastert, P. J. (2009). A new set of small, extrachromosomal expression vectors for Dictyostelium discoideum. *Plasmid* **61**, 110-8.

Vieira, O. V., Bucci, C., Harrison, R. E., Trimble, W. S., Lanzetti, L., Gruenberg, J., Schreiber, A. D., Stahl, P. D. and Grinstein, S. (2003). Modulation of Rab5 and Rab7 recruitment to phagosomes by phosphatidylinositol 3-kinase. *Mol Cell Biol* **23**, 2501-14.

Wang, X., Zhang, X., Dong, X. P., Samie, M., Li, X., Cheng, X., Goschka, A., Shen, D., Zhou, Y., Harlow, J. et al. (2012). TPC proteins are phosphoinositide- activated sodium-selective ion channels in endosomes and lysosomes. *Cell* **151**, 372-83.

Weiner, A., Mellouk, N., Lopez-Montero, N., Chang, Y. Y., Souque, C., Schmitt, C. and Enninga, J. (2016). Macropinosomes are Key Players in Early Shigella Invasion and Vacuolar Escape in Epithelial Cells. *PLoS Pathog* **12**, e1005602.

Wiegand, S., Kruse, J., Gronemann, S. and Hammann, C. (2011). Efficient generation of gene knockout plasmids for Dictyostelium discoideum using one-step cloning. *Genomics* **97**, 321-5.

Wilczynska, Z. and Fisher, P. (1994). Analysis of a complex plasmid insertion in a phototaxis-deficient transformant of Dictyostelium discoideum selected on a Micrococcus luteus lawn. *Plasmid* **32**, 182-94.

Yamamoto, A., DeWald, D. B., Boronenkov, I. V., Anderson, R. A., Emr, S. D. and Koshland, D. (1995). Novel PI(4)P 5-kinase homologue, Fab1p, essential for normal vacuole function and morphology in yeast. *Mol Biol Cell* **6**, 525-39.